POLITECNICO DI MILANO
School of industrial and Information Engineering
Master of Science in Materials Engineering and Nanotechnology

POLITECNICO
MILANO 1863

Charge density fluctuations: determination of their energy from the RIXS spectra of Cuprates

Supervisor: Prof. Giacomo Claudio Ghiringhelli
Assistant Supervisor: Dr. Riccardo Arpaia

Candidate:
Bruno Distefano, matricola 920854

Academinc year 2020-2021

A qualcuno...

Contents

List of Figures

Acknowledgments

Prefazione

Gli scienziati che studiano i superconduttori ad alta temperatura appartenenti alla famiglia dei cuprati al giorno d'oggi devono confrontarsi con la sfida del formulare una teoria miscoscopica capace di mettere insieme tutti quei fenomeni interagenti fra loro che competono o facilitano l'instaurarsi della superconduttività nei cuprati. Fra questi fenomeni un posto di primaria importanza è occupato dalle eccitazioni collettive raggruppate sotto il nome di 'charge order'. Le proprietà delle 'charge density waves' e delle 'charge density fluctuations'(CDF) si sono dimostrate una possibile causa delle comportamento anomalo del cuprati nella regione denominata 'strange metal'. Per ottenere una relazione fra i fenomeni che compongono il 'charge order', che coesistono e definiscono il diagramma di fase, molti modelli sono stati inventati e poco a poco perfezionati. Questa tesi, dopo aver portato un breve compendio sulla stato dell'arte dei cuprati, del RIXS e del 'charge order', ricava i valori dell'energia delle CDF e la loro evoluzione in temperature e doping. Per far ciò è stato necessario impostare un processo sistematico necessario all'allineamento dei set di dati ottenuti tramite RIXS da un campione leggermente dopato di NBCO e un'altro perfettamente dopato, analizzati in un ampio intervallo di temperature. I diversi passaggi del processo saranno discussi, porgendo attenzione alla loro validità ed efficacia, infine i risultati dell'analisi sono riportati e collegati all'attuale evoluzione del settore.

Abstract

The scientists studying cuprates high temperature superconductors nowadays face the challenge of formulating a microscopic theory able to bring together all the interacting phenomena that compete with or ease the way of superconductivity in cuprate compounds. Among these phenomena a place of primary importance is occupied by the collective excitation grouped under the name of charge order. The properties of charge density waves and charge density fluctuations (CDF) have proven to be likely the cause of the strange metal behavior of cuprates. In order to obtain a relationship between the charge order phenomena, that coexist and shape the phase diagram, several models have been invented and slowly perfected. This thesis, after bringing a brief compendium of the state of the art of cuprates, RXS and charge order, deliver a calculation of the energy of CDF and their evolution in temperature and doping. To do so a systematic way to align the data set obtained by RXS from a specimen of underdoped NBCO and another optimally doped, analysed across a wide range of temperatures, had to be developed. Several steps will be discussed pointing out their validity and effectiveness, finally the results of the analysis are shown and linked to the current hypothesis in the field.

Chapter 1

Introduction

After the advent of superconductors, both the industry and the research teams worked to increase our understanding of the phenomena that where behind it. The great advantages that this new discovery brought forth was the capability of these materials to conduct electricity in an environment virtually 'friction free'. This is due to the steep decrease of the electrical resistivity that a material capable of superconductivity undergoes when the temperature is brought below its transition temperature (T_C).

In fact, going under this temperature allows the atomic structure of the material lattice to rearrange itself in new configuration that, at first glance, appear to bend the expected physical characteristic. This is not true of course and numerous models arose as the researchers started to gain interest in the field. A prime example of this would be the Meissner effect [75] that through its later interpretations and application [102]) was able to offer an initial formalization of this new behavior.

After the initial discovery in 1911 [84], for an initial period it was thought that the superconductive dome of materials couldn't survive at temperatures above 30K. This theory was surpassed only when new materials able to reach and cross that limit were discovered [15] [117], and the era of high temperatures superconductors (HTSC) could finally begin. Following suite new materials were found year after year, pushing a new generation of scientists to modify the existing theories to adapt to the new data that flooded their field.

At that point the main limitation were the incredibly low temperatures required for a given material to superconduct. Overcoming them was and is a necessary step for bringing this new technology outside of laboratory application into day to day use, since maintaining temperatures hundreds of degrees below zero requires the employment of cooling liquids such as liquid

nitrogen that cause important expenses.

In this race a promising position was rapidly occupied by a class of HTSC know as cuprates whose structure, that will be described later in this document, shows a mix of exotic properties that have intrigued scientists all around the globe for a generation as of today.

Hand in hand with these new materials new probing techniques were developed such as angle resolved photo-emission spectroscopy (ARPES) and resonant inelastic x-ray scattering (RIXS), alongside the improvements on the already existing neutron scattering. This allowed the facilities that managed to put their hands on these top-notch spectrometers to observe these materials from a perspective that wasn't accessible before.

As it is often the case with every jump forward not everything was possible right away, the machinery had to adapt to challenges, both foreseen and not expected. This spaced from the need for new models for the analyses of the data to the inability of the spectrometers to probe excitations hidden in energetic jumps hard to distinguish or even register.

Examples of this can be found throughout the researches performed by the team of Prof. Ghiringhelli et al., that probed several families of cuprates in search of a new understanding on the interactions between superconductivity and the newly discovered phenomena denominated 'charge order'.

It is in one of these researches that this thesis work find its roots. In the second chapter I will covers the properties of the cuprates, their electronic structures and their phase diagram, explaining how the latter is subdivided and what are the properties of each region that compose it.

In the third chapter I describe the spectroscopic technique of Resonant X-ray scattering (RXS) from its origin through its development, covering the models employed during the year to read and model the data obtained with it.

Furthermore in the fourth chapter, to help the reader in acquiring a more roundabout view, I'll add a review of the discovery and evolution of charge order. It will stem from the early signs of striped order and it will cover the several variations that were observed in the cuprate families, to end in the recent discoveries of charge density waves (CDWs) and charge density fluctuations (CDFs).

Finally, having covered all the basis, the fifth chapter is focused on the description of the work. I will explain the meaning of the data analyzed, the boundary set and the steps followed in search of a repeatable process that could allow to better read information often hidden behind a lacking experimental resolution. The limits of experimental resolution are in fact a problem that periodically reappears. Since when a new probing technique

appears, or a classic ones it upgraded, what was before hard to see becomes easier, and new questions arise where there weren't before.

In this thesis several data set from an experiment conducted on NBCO specimens [9] were analysed. A punctual alignment procedure divided in steps, allowing for a progressive improvement, was adopted and employed. This was done hoping to get to a results, centered on the region mostly influenced by CDFs and consistent with a proposition on the evolution of the behavior of the CDFs, that was not possible to read before the alignment.

And while this study alone is in no way a definitive proof neither for the equation proposed nor for the behavior it describes, it serves as a tool that was able to achieve a clear image were there was only a speculation. A tool that can, while lengthy, easily be applied for different electronic excitation and that could, adapted to the situation, enable to create a proof from a data-set that wouldn't otherwise allow for it.

Chapter 2

State of the art of Cuprates

2.1 Cuprates lattice and electronic state under doping

In this chapter I'll give an explanation of what are superconductive Cuprates, to do so I'll define the properties and peculiarities that lead the analyses down the line.

Cuprates are basely a class of materials containing in their structure molecules of copper oxides. The variety I will consider branches from a semi planar structure of layered CuO_2 and metal oxides acting as charge reservoir [103] (figure 2.1). These materials, at room temperature and undoped, behave as long range antiferromagnetic charge-transfer insulators. But, given the right doping and temperature condition, can transform into superconductors. [85]

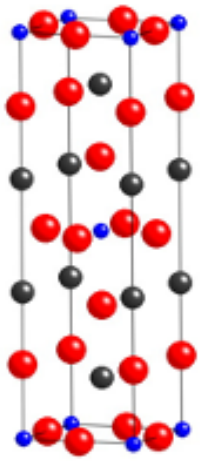

Figure 2.1: LBCO; copper (blue), Oxygen (red), Lanthanum (dark grey) [36]

The first appearance of this kind of structure dates back to 1986 when Bednorz and Müller achieved superconductivity in a Lanthanum doped Copper Oxide. [15]

The unit cell consists of three perovskite cells on top of each other. *Each perovskite unit cell contains a metal atom at the center: one in the bottom and in the top unit cells, a different one in the middle one. Cu atoms occupy all the corner sites, while oxygens are placed in the middle edge positions. The CuO_2 planes are located right above and below the metal ion.* [89].

Responding to its first appearance a number of researches focused on this novel material and ultimately lead to a bloom in publication and a Nobel prize for Bednorz and Müller. As a consequence of this increased interest in the field a considerable number of new structures were created and their properties studied extensively (figure 2.2). It was decided to divide all these new materials in 5 groups [103]:

- Lanthanum barium Copper Oxide (LB-CO)
- Yttrium Barium Copper Oxide (YB-CO)
- Bismuth Strontium Calcium Copper Oxide (BiSC-CO)
- Thallium Barium Calcium (TBC-CO)
- Mercury Barium Calcium (HGBO-CO)

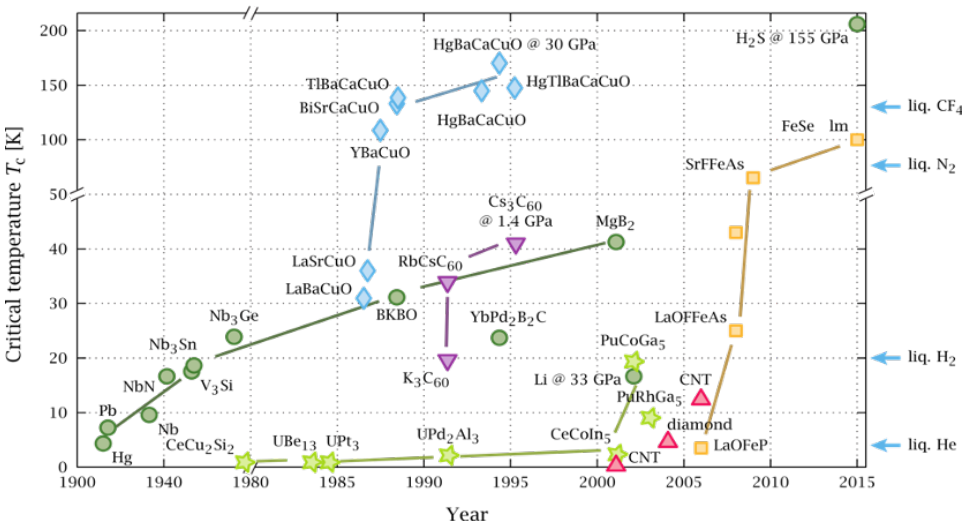

Figure 2.2: Superconductor's timeline, Cuprates in light blue [88]

A configuration of the layered structures common across the different families shows CuO_2 planes alternated with one or several layers where the copper is replaced with a specific metal ion. This ion is usually what defines the family of the component.

These inter-planes act both as charge reservoir and as doping wheel for the copper oxide planes, enabling as such both positive and negative doping. This is in fact influenced by the amount of Oxygen that element chosen may bind.

The copper oxide plane can be seen as a square lattice where every cell contain one hole $d_{x^2-y^2}$ orbital. The hole concentration can be changed to avoid the energy tool caused by having two positive charges in the same state[31]. That's because the unit square planar cell of CuO_2 contains an odd-integer number of electrons whose movement is energy expensive (energy gap of 2eV) causing a "traffic jam". A proper doping level can reestablishing a Fermi liquid state at low enough temperature and high enough magnetic fields [67].

This sectorialization and periodicity of the crystal structure acts as a spacer for the electronic properties resulting in the presence of only a weak coupling among the CuO_2 layers. As a consequence there is a strong anisotropy characterised by great conductivity in the copper oxide layer while showing considerable obstruction if the tests are done in the perpendicular direction.

2.2 Phase diagram

2.2.1 Phase diagram composition

As previously stated, under no doping condition these materials behave as Mott insulators, following the band theory and showing a gap in the d-orbitals at sufficiently low temperatures. But this changes under doping and the structure rapidly modifies its properties entering in the superconductive dome.

This behaviour is quite peculiar since typically *magnetism arises from strong repulsive interactions between electrons, whereas conventional superconductivity arises from induced attractive interactions, making magnetism and superconductivity seemingly anti-thetical forms of order* [67]. As a consequence the classic BCS theory of superconductivity based on the formation of Cooper pairs with energy under the phonon energy doesn't work for these materials.

As it became public it defacto put the cuprates in an odd position, position that now we know is called *strange metal*. And as a number of materials joined the group alongside them [108] it become apparent they were related mostly by the strong correlation inherent to their own electronic systems. Add to that the unclear events unfolding right before getting down

to T_C and we have all the ingredients for a new field of research, filled with an abundance of phenomena to name.

And physicist ran to it and naming they started, this grey area above the T_c was named pseudogap regime... and that's about as far as it was clarified about it as many of its properties remain a mystery for the most part even now. What is tough speculated is that is in this pseudogap that a number of ordering phenomena arise, and they are of primary importance in our understanding of cuprate superconductivity. I'll focus hereinafter to what is known as charge order.

This ordering phenomena, while not theoretically unseen [46], were experimentally unknown. Their presence caused the formation of a superlattice causing a novel gap in the superconductive state unseen in the classic s-wave superconductors.

In order to understand, or at least make solid hypotheses on their microscopical properties, it is useful to break down the phase diagram of a typical Cuprate. Then each domain can be considered separately, showing how one evolve into another and what changes during these transitions.

This is particularly necessary since Cuprates are bearers of a particularly articulated phase diagram composed of a number of different regions, some of which intertwine to manifest unexpected and sometimes unclear behaviours.

Let's make a step back and define what a superconductive phase diagram is. The phase diagram is a 2D plot showing temperature (in K) on the y axis and doping level on the x axis.

It is used to track the phases that some materials alternate during doping and/or thermal cycles. From it's early age studies followed on every element and compound worth studying and a number of phase diagram arose. Each and everyone slightly different from the others, some for different bounds in the T_C or in the doping level, others presenting entirely new phases not studied before. This would be the case for the phase diagram of the cuprates that have been refined for years and now presents itself with a plethora of phases (figure 2.3) [74].

Here we can see a number of different domains have claimed their share of the diagram, and some end up trespassing into others.

Just as useful is realise the different behavior observable in different sections of the diagram:

- on the rightmost side of the diagram we can observe the overdoped regime at $p > 0.16$ where the strange metal makes way for the Fermi liquid of quasi-particles.

- the optimally doped region resides at the center of the diagram, in the

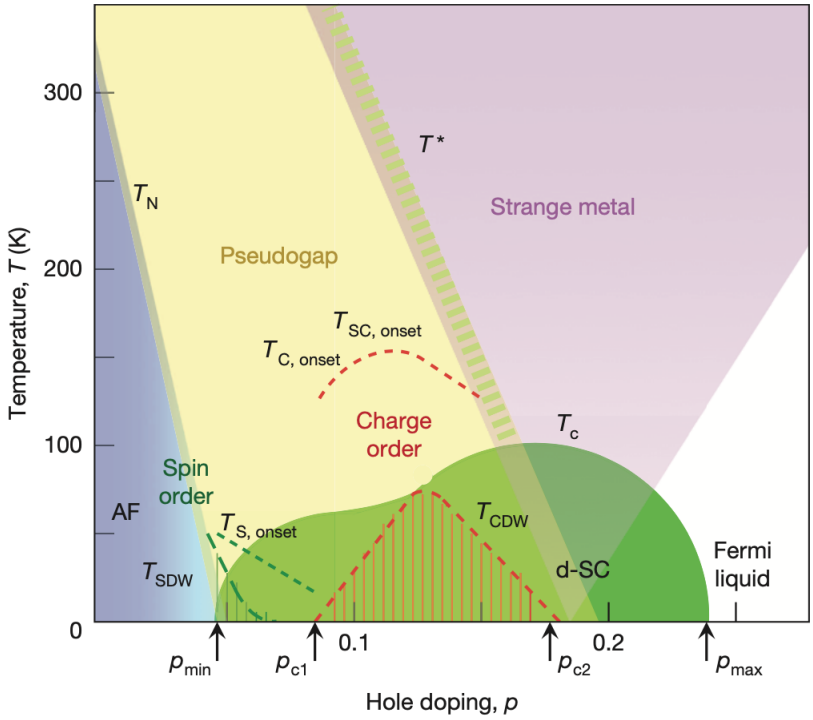

Figure 2.3: Cuprate phase diagram [67]

region around p=0.16, is a domain permeated by the strange metal behaviour. In it resistivity changes linearly with temperature well beyond room temperature, character denominated "Marginal Fermi Liquid" [108].

- all that remain is the underdoped portion of the phase diagram at $p < 0.16$ and it is the most interesting since it is, alongside the antiferromagnetic region, the habitat of the pseudogap and of a number of exotic ordering phenomena.

- the superconductive region span over most of the doping evaluated range and cross path with several of the aforementioned regions.

2.2.2 Pseudogap

In order to delve a bit deeper into charge orders an excursus on the pseudogap region would be of use. The pseudogap is the yellow region (figure 2.3) on the phase diagram, spacing manly is the underdoped region all the way to the optimally doped mark. It was firstly foreseen by irregularities

in the low-frequency spin excitations [115] and promptly confirmed by reflectance measurement on the gap lowering conductivity of $YBa_2Cu_3O_{6+x}$, at different x values (0.6 and 0.95) to pinpoint its presence.[63]

Looking at the electronic excitation of the nodal region along the diagonal directions of the layers we find a considerable suppression in the spectral weight of low-energy excitations, these exact range is what today we know as the pseudogap. [30].

Moreover here the Fermi surface doesn't maintain the postulate of continuity presenting "Fermi arcs". The Fermi arcs are discovered by cooling samples from above to below their T_C and looking through Angle Resolved Photoemission Spectroscopy (ARPES) at their nodal region momentum space. This way it was found that the Fermi surface opens up at a temperature T^* into disconnected arcs that eventually collapse into the superconductive ground state at the nodal point at T_C. [80] (figure 2.4).

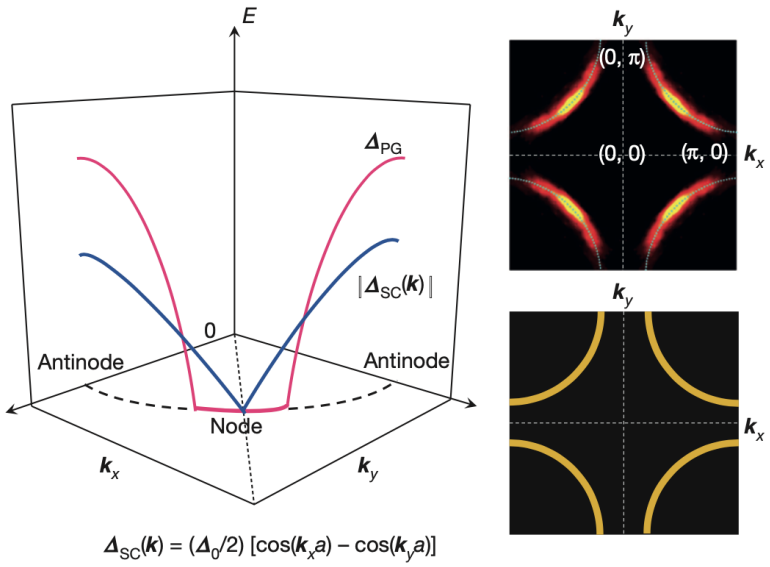

Figure 2.4: Fermi surface, Fermi arcs and gap functions as found by ARPES ans STS for overdoped compound (lower right) when the pseudogap sets in (upper right) with the difference between the nodal and antinodal region highlighted in momentum space (on the left) [67]

These gapless arcs are deemed to be merely an intermediate state in the transition of the d-wave pairing correlation's nodes into a Fermi surface that happens when moving from below to above T_C. What's interesting is why this intermediate states appears and what influences it, since this "unusual behaviour, where the Fermi surface does not form a continuous contour

in momentum space as in conventional metals, is unprecedented in that it occurs in the absence of long-range order" [80]. Furthermore it presents with a difference in temperature dependence between the pseudogap and the superconductive dome implying at some different precursors. This difference isn't limited in temperature evolution since it differs further at different k values in the momentum space [80].

Multiple theories have aimed at giving a clear understanding on how the reconstruction of the Fermi surface undergoes with variable degrees of effectiveness, among them a prominent idea have risen from the mean-field theory. This theory predicts that the pseudogap could be the work of a charge density wave creating surface pockets. To prove this studies have been undertaken trying to confirm that this Fermi arcs are a side of those pockets by finding the backside of it, proving though non conclusive [121] [72].

This remains to date a complex domain with a number of open questions since experiment performed with ARPES [80] and STS [113] over the years have found inconsistent results in the antinodal region, leaving the exact properties of this charge order still under debate [33].

Since this pseudogap is present only in the antinodal region [40] [70] where the the d-wave gap is the larger: it is likely that pairs forms already at T^* but are impaired to actually cause a superconductive state by a phase fluctuation [67]. These hyphotesis would suggest that the charge order could be heavily influenced by charge ordering phenomena and that these phenomena could both intertwine with superconductivity and appear over a wide range of temperatures, both above and below T_C.

This correlation between the pseudogap region and the superconductive dome, considered all the information and open question here reported, has lead to an advancement of interest over the Charge order.

2.2.3 Charge Order

Charge order is a 2D or 3D phase shift caused in strong correlated systems such as Cuprates, leading either to a disproportionation of atoms in the lattice or to the creation of a superlattice. Charge ordering phenomena have first been discovered in Cuprates by neutron scattering experiments on underdoped LSCO in the form of stripes [105]. These stripes appear as a consequence of the competitivity between doping induced phase separation and long-range Coulomb interactions [42].

These stripes, pinned down by the tetragonal lattice deformations [105] and of short range [118], held a metallic behavior and superconduct at low

temperature much like a partially crystallised superconductor [35] [93]. They forms pair density waves that are superconductive in nature but with an opposite phase from one stripe to another (figure 2.5) presenting an hourglass pattern in momentum space [8]. This behavior was initially shown on samples of doped $La_{1.6-x}Nd_{0.4}Sr_xCuO_4$: at a hole doping near 1/8 they change from a low-temperature orthorombic (LTO) to low-temperature tetragonal (LTT). This change in lattice configuration, along the dopant concentration and below T_C temperatures, caused a suppression in superconductivity. The fact that "the suppression occurs when the hole concentration is close to a simple fraction suggests that a commensurability effect is involved" [106] potentially allowing for long-range order. The 90° rotation is caused by the atomic displacement pinning of the lattice, basically causing a charge and spin coherent modulation where the greyed layers are caused by the holes segregation [106].

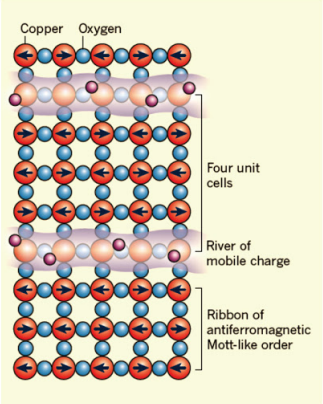

Figure 2.5: Stripe-like electronic order in high T_C cuprates [46]

From this first discovery others followed in other families of Cuprates [119] [101], but a coherent model for striped order wasn't found in all specimens.

An important development was brought forth by Ghiringhelli and his colleagues on the competition between superconductivity and charge order studying $(Y/Nd)Ba_2Cu_3O_{6+x}$ specimens [50]. They found out a new type of charge modulation, unaffected by spin and incommensurate; more on this later.

2.2.4 The strange metal

In the middle to high doping section of the phase diagram, above T^*, we find ourselves looking at a region called of the strange metal.

As the name implies this region is characterized by a peculiar dependence of the resistivity on the temperature, that rather than increasing to a plateau up to melting point (when the mean free path becomes of the order of the de Broglie wavelength) [67, 11, 114], changes linearly with temperature up to temperature much higher than room temperature [73]. Differences that are transferred to the Hall resistivity temperature dependence that differs from what quasiparticle behaviour would have caused [32].

A theory arose to collect these and others abnormalities under the name 'marginal Fermi liquid' [108]. Alongside that it was theorised a quantum critical point (QCP) that sets apart ordered and disordered quantum phases. This permitted to build a justification for the low energy excitation in the strange metal while denying the presence of quasiparticles in it.

The QCP, while working in some scenarios, have serious limitation. They should be intrinsically unstable and as such always covered by the superconductive dome, but that can't be true. Moreover it should follow the pseudogap at temperatures well above its theorised maximum. This leaves the QCP as a work in progress theory that now is being studied by string theory and holographic model scientists [45, 39].

2.2.5 The overdoped regime

To complete the overview of the phase diagram we have to look at the rightmost region, at a doping level of $p > 0.16$, this is the overdoped region. This region ranges from the right side of the superconductive dome up to the Fermi liquid region. It's a domain where the classic properties described by the one electron band theory [112] properly describe the Fermi surfaces throughout the Brillouin zone [30]. Here an almost quadratic dependence of the resistance on the temperature is restored [12]. Some spin fluctuation though persist even in highly doped cuprates [38].

Chapter 3

RIXS overview

In this chapter I will explain the experimental technique which is central in this thesis. I'll start with a brief introduction of the physical principle and follow up with an in depth look at the facility that made it possible.

3.1 X-ray spectroscopy

To investigate the properties of a material, both at the micro-scale and at the nano-scale, one needs the usage of an input and the collection of an output. The interaction of our input with the material causes a modification of some of the bulk properties of the materials. The output signal will therefore depend on these properties, and its study will therefore provide information on the material.

At the nanometer scale, when entering the quantum realms, looking at particles and material properties is very hard. Scientists have found in microscopy and diffraction analysis powerful tools that allow them to observe the atomic lattices by the energy exchanged by their electrons during their allowed transition. The former method is used for direct space tests, while the latter is preferred for the indirect space ones.

The main medium of observation relies on the use of the fundamental particles composing the atoms, namely electrons and neutrons, or photons.

Each method has its advantages and cons. Electron beams shines in definition and are easy to create but are not of much use to study the properties behind the outer layers, since are lacking in energy. Neutrons, being way less interactive with the electrons of the samples, can travel much further and interact mainly with nuclei, this makes them a better choice for studies focused on magnetic properties. On the downside a neutron beam is hard to produce and is characterized by a very small scattering cross section,

which limits the investigation to bulk samples having large volume.

Finally photons shows a number of optimal properties: they are easy to produce through lasers and playing with their wavelength a number of different rays can be output from our source. Moreover, because of their scattering cross sections, a rather intense output signal can be obtained even from very small samples, e.g. thin films. Among the viable options, X-rays became recently predominant in spectroscopy and energy loss analysis: indeed, they are able to stimulate phonons and interact with both atomic orbitals and atomic spins, thanks to the presence of spin-orbit coupling[25].

3.2 Resonant Inelastic X-ray scattering

3.2.1 RIXS origins, pros and cons

The problem when we look at complex systems such as cuprates, is that a number of properties superimpose and intertwine in their response to an input. This makes the task of deciphering how each one behaves rather complex.

In fact we have to take into account the orbitals, the density of states (DOS) of valence electrons and the spin momentum, on top of the crystalline structure. For the case at hand the cuprates are among the 3d transition metals (3dTM). As such they have an half filled shell that is atomic-like enough to lead to strong correlation and localised magnetic momentum, but radially expanded enough to form stable covalent bonds. This translate in the presence of a relevant hopping integral and of superexchange interaction conveyed by the Oxygen [25].

X-rays spectroscopy is a good candidate for studying them but lacks in resolution, therefore a new method was developed as an evolution of a Raman spectroscopy. A Raman process sends out an electromagnetic monochromatic wave that excites a core level causing the formation of an apparent momentum. The material output wave mainly follows an elastic path, giving back Rayleigh radiation with the same frequency of the incoming laser. The energy of the jump can now be extracted as the difference between the input and output radiation as a consequence of the conservation of energy:

$$\hbar\Omega = \hbar\omega - \hbar\omega'$$

Adding to that a typical Raman spectra shows signs of inelastic interactions emitting what are called stokes or anti-stokes waves at diminished or increased frequency respectively. This happens since the excited electrons

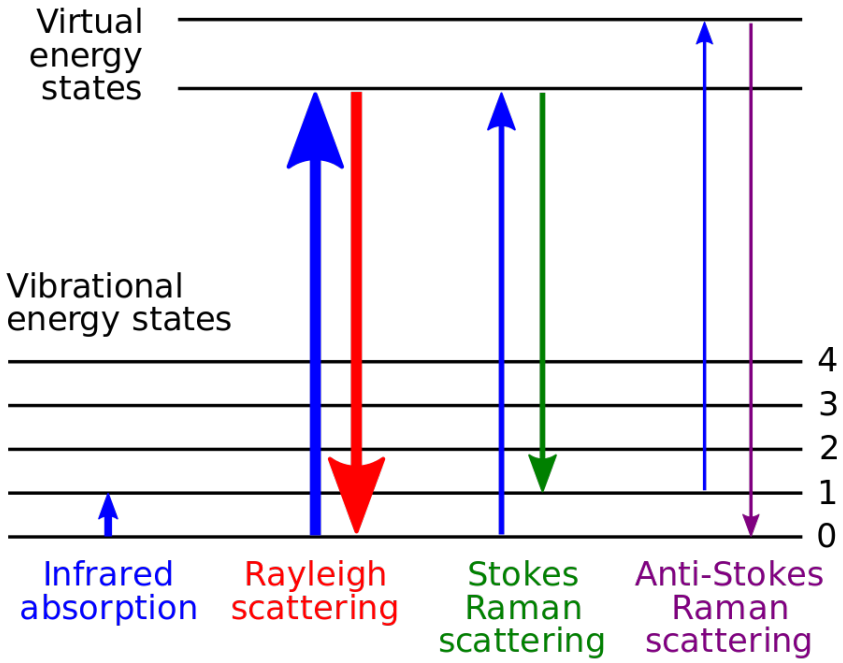

Figure 3.1: Scheme of Raman elastic and inelastic excitations [78]

relapse back into a level that's either more or less energetic than the original one (figure 3.1).

This technique is widely used and offers a number of advantages, but lacks in resolution. Generally speaking we can think of resolution as the precision of details that an analysis offers. This is hindered by the presence and influence of broadening or shifts in a spectral lines, each creating artefact in what would otherwise be a perfect spectral line shape. These phenomena can be caused by both local and/or extended conditions, and either of them can be dived further down to a number of more precise conditions.

Among these, the natural local broadening of a curve is heavily influenced by the lifetime of the excited state of an electron undergoing a two phase transition. The broadening is justified by the uncertainty principle stating that the energy of a state gets more and more blurred in time since it may or may not have undergone spontaneous radiative decay or Auger processes [49].

One of the main advantages of a resonant technique is that a high energy core-hole is absent in the final state leading to intrinsically sharp spectra with energy and momentum resolution determined by the instrumentation [5] [96]. RXS presents different challenges such as the availability of a precise

monochromator and energy analyser and the precision needed in the setup of the energy range. In addition resonant process are usually weak and comes with a small cross section needing thus a high-brilliance x-ray source. All of this adds up to only a small number of facilities performing these type of procedures and all of them being synchrotron facilities.

These inconveniences are nonetheless faced since the results are worth the extra miles, they in fact not only offer a much greater resolution than standard x-ray spectroscopy, but allows to analyse a number of properties of selected samples [6].

- As a technique that employs x-rays, RIXS can use its wide range of energy tuning allowing as such to observe all the way down to low-energy excitations in solids.

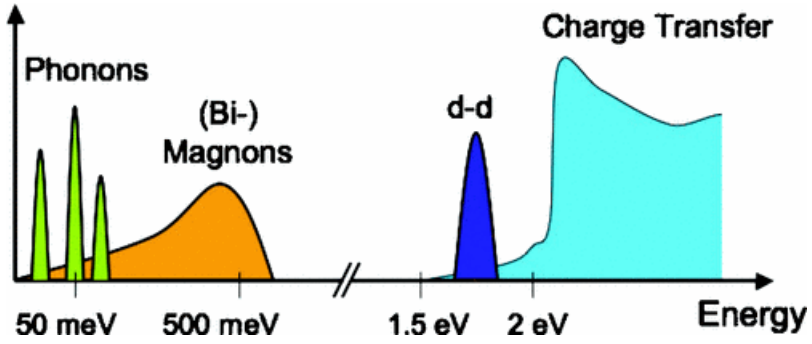

Figure 3.2: Approximated energy scale of elementary excitation in metal oxides [6]

- It is moreover possible to distinguish not only different atoms, but same atoms forming different bonds as well. This is allowed since the incoming radiation is tuned to the exact energy needed to promote a specific core level to the Fermi level. This enable to differentiate the different transition the same element's electrons can undergo. The fact that each of these transitions have its own absorption edge is what makes it resonant.

- It is a bulk sensitive method since it can use both hard x-rays ($\approx 10keV$) with a penetration depth of few microns and soft x-rays ($\approx 1keV$) lowering it down to around 0.1 microns (perfect probe for the Cu L-edge).

- It can give results with samples in the nanometer range since it emits much more photons than a neutron source and interact just as much more with the sample's matter.

- It is able to provide information on Charge Order [97].
- Finally, is a technique that can disentangle the different components previously stated that partake in an excitation event. This feat is accomplished by polarising the scattering photons to backtrack the symmetry and nature of an excitation. This is a complex procedure and not too many experiments have been performed [23].

This last point in particular is possible since x-rays add the momentum conservation to the energy conservation law extracting the momentum transferred from the wave vectors **q** again as a difference between the input and the output:

$$\mathbf{q} = \mathbf{k}' - \mathbf{k}$$

And if the materials presents an homogeneous lattice without different grains or domains that momentum can be precisely connected to a unique point in the reciprocal space of our specimen.
$F_{fg}^{indirect}(q,w) = P(w_k, w_{k'})T(\epsilon,\epsilon')\langle f|\rho_q|g\rangle$ [1] [2] [3]

3.2.2 RIXS instrumentation

As previously said one of the main point for the success of RIXS over other techniques is the improvement of the experimental resolution [57]. In particular I'll explain how it is driven by the instrumentation.

A proficient and clear analysis over this topic was provided by professor Ghiringelli and professor Braicovich[25]. When a RIXS system is projected a fine tuning has to balance the high energy resolution desired with the count rate on the detector. The first problem arise since low frequency high wavelength x-rays are hard to be monochromatised. Furthermore a simple Bragg analysis of the results is not trivial either since it is hard to create a single crystal with a lattice unit wide enough for the task. Add to this the fact that only a limited number of layers can participate in the Bragg reflections, since the absorbance of each one dissipate the signal quickly, and we obtain a signal with considerable rocking curves.

The solution found was to use diffraction gratings (with up to 1600 slits/mm in high resolution tests) at grazing angles. The beam must be of high quality on itself and its generated at dedicated beam lines by long (4–6 m) undulators of 3rd generation synchrotron radiation storage rings [25].

[1] $P(w_k, w_{k'})$ is the resonant function
[2] $T(\epsilon,\epsilon')$ is the polarization dependence
[3] ρ_q is the density operator

The beam, after being polarised by an ondulator, undergo a set of mirrors and a monochromator to have its band wide severely reduced, typically to 10-80 meV in the 450-900 eV range. Once that is achieved the beam is focalised on a rectangular region of the sample with dimensions in the hundreds of microns or lowers. The beam can deliver up to 10^{12} photons per second, and the rebound beams are handled by one or more mirrors to be delivered to a photo-diode or to a Charge-Coupled Device (CCD) for mapping.

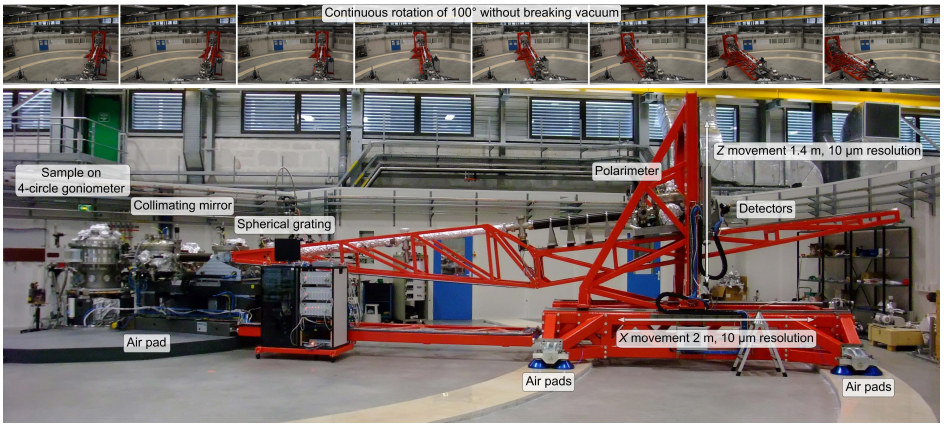

Figure 3.3: RIXS beamline at ID32 [44]

The first point of attrition towards an increase in resolution is in the arm length of the monochromator: a major distance could best differentiate the angular resolution at the final screen. The distance slowly but steadily increased from 50 cm in the first experiments performed in the 90' [79] upward until in 2015 a new record was set at the ESRF in Grenoble for its ERIXS setup at site ID32 [28]. There the monochromator arm length reached 11 meters, managing a resolution of 35 meV at the Cu L_3 edge (25 meV in its most recent upgrade [44]). This was achieved making use of a massive collimating mirror with an ability to gather the scattered particles down to a precision of 20 mrad (figure 3.3).

Finally, is necessary to take into account some closing points: the precision of the sample's vertical spot, the necessity to create a system both mechanically and thermally stable and the detector's spacial resolution [7] whose efficiency has to be balanced with the ability to collect data about the beam polarization [24].

I'll now briefly cover the main excitation that have been covered by RIXS up to date.

3.2.3 Charge transfer excitations and edge specific case history

Being RIXS able to not only analyse the momentum dependence of charge transfer phenomena, but do this under extreme pressure in their energy scale [91], it was extensively used to characterise metal's K- M- and L- edges as well as Oxygen K- edges. These excitation can be either direct or indirect and generally adhere to the following scheme (figure 3.4):

a a core-hole is created in the metal

b charges from the ligand site rush to screen it until the core-hole decays

c the spectator decays as well

d some charge rearrangements can held, fixed in place, causing charge transfer

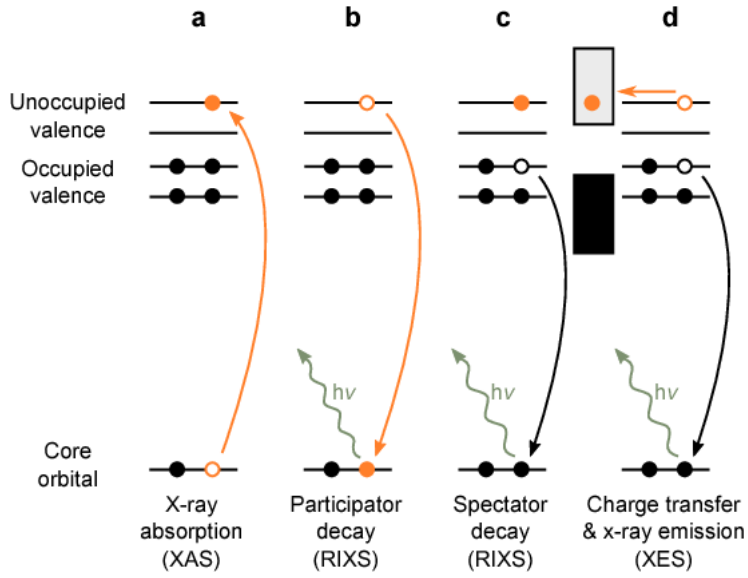

Figure 3.4: Model of charge transfer excitations

Chronologically the first RIXS analysis for charge transfer were performed at the K- edge of NiO in 1996 [66]. Platzman and Isaacs rapidly followed with a study of $NiSi_{1.5}Se_{0.5}$ [87].

From there we can see the appearance of cuprate compounds (Nd_2CuO_4) [61], and just one year after it was made clear that the results were in fact charge transfer excitations [3].

For the cuprate case a better model involves the formation of an intermediate state at the core-hole that steals an electron from a nearby atom creating a two-hole state known as a Zhang-Rice singlet (ZRS) [6] [109]. This process can cause dispersive features in the lattice after it settles.

Different is the case for the L- edge where the core-hole is screened by the same electron that goes excited. No screening comes for nearby atoms contribution and the jumps are expected only among bonding and anti-bonding metal states. This is more evident if the beam targets the weak satellite features above the main absorption edge. Here we observe an higher ligand character and a considerable overlap with similarly ligand states. Non-bonding states were observed as well at energy of 5-10 eV for TiO_2. [56].

The approach changes slightly for the M-edge where the charge transfer excitation were found on a study on CeO_2 and UO_3 at the Ce and U M-edges via the use of the Anderson impurity model. [29].

Finally the Oxygen K- edge is of somewhat secondary relevance. A case history saw it adopted to study a $Sr_2CuO_2Cl_2$ sample [71], the study confirmed the ability of this procedure in obtaining data from low energy features. Other researches instead focused on analysis on double magnons features [41], dd excitation, non local screening, and bonding-antibonding transitions [110]. Some went as far as theorise the possibility of making use of the momentum dependence [83], that was indeed subsequently used to differentiate states near precise symmetry points [69].

3.2.4 dd excitations

In order to study some phenomena we have to look at dd forbidden transitions. These are orbital excitations representing a change in the symmetry of the occupied Cu-3d states, sometimes violating Fermi selection rule. Such excitations exhibits energy usually around 1.9 eV and always above 1.5 eV [92].

The first correlation of dd excitations with superconductivity was theorised when relation between the Cu to apical-oxygen distance and T_C was found several years ago [82].

These jumps can be observed by RIXS since they are split into two consecutive dipole transitions. For example at the L_3 edge a $2p_{3/2}$ electron jumps to a 3d shell absorbing an x-ray photon and putting the system in a highly excited state with a deep core hole. Afterward the system decays when a 3d electron falls back into the $2p_{3/2}$ states releasing a photon [92].

The study of dd excitations can be approached both by direct and indi-

rect RIXS. In a direct RIXS the excited electron of the ground state remains highly correlated to the core-hole formed in its stead and thus doesn't delocalise, up until it falls back into the core state. This has been measured from early transition compounds [23] to cuprates [51] [22].

And has been confirmed by a study conducted on TiO_2 [56]

Making a striking comparison with a similar non resonant process (IXS) [68] we can observe the difference in resolution. Where a RIXS calculate the final amplitude as a combination of the amplitude of two separate processes, the IXS does the same but with an exponential expansion of the spare of a singular amplitude. This impose on the latter the calculation of only even operators [111] thus causing the processes to undergo different symmetry transitions due to different selection rules. This translate in more noisy results for the IXS [59] and makes RIXS the more precise approach.

If the approach followed instead the path of an indirect RIXS we would often observe an hybridization of the 3d shell with the 4p [55]. For this scenario we would want to extract an effective transition operator from the indirect RIXS equation previously reported.

The results obtained from direct and indirect procedures present some differences: from the latter an electron operator pops up while the former shows a hole operator, furthermore in the latter an extra constant appears in the resonant function. This still leads to the same final one-particle tensor operator and angular dependence [6].

More recently, in order to comprehensively studying the cuprate dd excitations a team used RIXS to study several samples with an experimental resolution as high as 130 meV [92]. The study treated the scattering ion as a hydrogen-like system of a single hole and reformulated the one-particle wave-functions in spherical harmonics of the angular component. This was possible since all the transitions share the same radial component and the single 3d hole present in the ground state has an almost pure x^2y^2 character. The spectra were then calculated thanks to these simple harmonics and fitted to the theoretical models.

The results showed that while a constant field (CF) model can get close to the power law dependence of the energy loss it neglects completely the Cu–ligand orbital overlaps. This implies that some important physical properties are totally missing such as the super-exchange interaction [92].

This model was then modified by treating the dd Coulomb and exchange interaction within full atomic multiplet theory and using symmetry-dependent Cu 3d–O 2p hybridization to describe photo-electron spectroscopic data, [43] getting results much closer to the experimental ones.

The study findings concluded that magnetic excitations (up to 250–300

meV) play a major role in Cooper pairing in cuprate superconductors since dd excitation are missing in the mid-infrared region. Furthermore it emphasised the importance of apical ligands on the dd even tough it could not find a clear predictive model.

3.2.5 Magnetic excitations

A normal inelastic neutron scattering transfers a spin=1/2, being able to modify the angular momentum by either 0 or 1. A RIXS process offers more variability with a unitary spin value that can create both single magnon and two-magnon excitations via the conservation of angular momentum [19].

Moreover this new technique, targeting a core-hole intermediate state, could make use of its strong spin-orbit coupling making for an easier transfer of angular momentum up to the tens of eV. The magnetic excitation can be probed by both direct and indirect RIXS.

A direct process targets typically 2p, 3p $\rightarrow$ 3d edges of Ni and Cu because of the large spin-orbit coupling of the 2p core-hole [27]. These edges spits into intermediate states where spin-flip processes can take place, unlike in optical spectroscopy. Contrary to theoretical expectations [52] the spin-flip transitions (for the $3d_{x^2-y^2}$ orbital) are experimentally observable also when the spin is parallel to the z-axis [20].

On the other hand a typical indirect process can be seen as a 1s $\rightarrow$ 4p where the the core-hole couple locally with the spin affecting the super-exchange interaction [19]. This jump allows for spin conservation ($\Delta S^z = 0$) with a coupling constant $J \approx 100$ meV, instead of the single digit values usually obtained when spin isn't conserved ($\Delta S \neq 0$). And since this doesn't commute with the magnetic Hamiltonian, magnetic exitations pops up.

For this type of analysis the RIXS intensity is made of a local structure factor influenced by polarization, geometry and excitation mechanism. It must be multiplied as well by the appropriate spin susceptibility [58] that depending on spin interactions can be featureless or heavily q-dependent.

Nowadays magnetic excitations have been observed with RIXS on many complex materials and structures ranging across 1D [94], 2D [20] and 3D systems [94].

3.2.6 Phonons

Finally we have to add phonons to the picture. Phonons are collective periodic excitations that, in a typical energy loss cuprate spectra, appears at energy between 0 and 90 meV [19][21][54].

What must be understood is the effect that electron-phonon coupling (EPC) has to the plot and to the physics behind.

The importance of it derives from the major role EPC has in the formation of Cooper pair in conventional superconductivity. In fact EPC induce charge density modulations and decisively influence the transport properties of materials [26].

But in cuprate EPC doesn't justify the high T_C and a lot of debate still hold in regard to their role. A leading theory would suggest that even a small amount of EPC could increase T_C of a fair amount [65]. In each case EPC affect CDW as well at both low [77] and high energy excitations [37].

This create a situation where understanding EPC is both important and hard since it is hidden behind strong electronic interactions [26]. In fact, understanding their influence would allow to better disentangle them from other parameters in the study of CDWs.

A first assessment of EPC was detected via RIXS [5], but was very limited to a specific category of materials [95].

A more recent study measured EPC via energy-detuned RIXS experiments comparing the incident phonon energy with available theoretical models. They managed to obtain an energy peak at the antinodal point that rapidly disappears at the BZ center [90].

The calculation made use of a model (analysis of which goes behind the scope of this section) that allowed them to extrapolate the momentum dependence of the EPC from the relative change of the phonon intensity as a function of momentum transfer [90].

A follow up to the precedent study deepened our understanding of EPC in cuprates considering more factors like effect of doping and momentum transfer [26]. This same study was able to confirm the symbiotic behavior of EPC and CDWs but wasn't able to discern if either phenomena was the cause for the other one.

The results obtained so far are important since they have demonstrated the cabability of RIXS in studying EPC in cuprates at different doping levels, but more researches ought to follow. The present constrains are imposed by the experimental resolution limits of the technology. This means that the improvements that will likely be reached in the next years will allow to further our comprehension of the phenomena itself and of its influence in the field of high T_C cuprates.

Chapter 4

Charge order in cuprates

4.1 The early age: from neutron scattering to resonant x-ray scattering

After having introduced both cuprates and resonant X-ray scattering techniques, here I intend to give an overview about charge order, a phenomenon which might be crucial to understand the still mysterious physics of cuprates, and whose detection and understanding relies on the development of the RXS techniques in the last 15 years.

A large variety of ordering phenomena have been found and studied in cuprates during the years, mostly concentrated in the underdoped side of the phase diagram. In first approximation, they could be divided in zero momentum order (Q=0) breaking rotational symmetry and finite-momentum order ($Q \neq 0$) affecting the translational symmetry. Charge and spin modulations are a typical example of the second kind [34].

Charge order first appeared in the form of stripes in the La-based cuprate family, where rivers of holes are separated by anti-ferromagnetic domains: here, a locking of magnetic and charge excitation is present. [34] Indeed, it was discovered first by neutron scattering on underdoped $La_{1.92}Sr_{0.08}CuO_4$ (8% hole doping) [122] and $La_{1.89}Sr_{0.11}CuO_4$ (11% hole doping) [17] and subsequently studied extensively. Different experiments on the field followed focusing mainly on the momentum structure of the incommensurate anti-ferromagnetic order and on its relationship to the ordering of the doped holes. From these experimental evidences, numerous models where constructed. The emergence of an incommensurate AF order within the superconducting phase allowed to pinpoint a possible interplay between short-range magnetism and superconductivity in the cuprates. [34]

The ground state of the stripes is characterized by short ranged, uni-

directional, charge modulations, separated by the magnetic domains, and whose wave vector is twice that of the incommensurate spin modulations. [123]

A similar stripe states reappeared other experiments [107, 105], confirming the wave vector relationship $\delta_{charge} = 2\delta_{spin}$.

Some years later, at the end of the 90s, the atomic resolution reached by scanning tunneling microscopy allowed the detection of density modulations with remarkably short correlation lengths.

This newly experimental capabilities were firstly applied at a sample of $Bi_2Sr_2CaCu_2O_{8+\sigma}$ (Bi2212), a similarly layered cuprate. This allowed the discovery of charge modulations, with a correlation length of 30 Å, at the same doping level investigated in the pioneering experiments on LSCO.

Spectroscopic measurements resolved as a function of sample-to-tip voltage brought to the discovery of quasi particle interference (QPI) on both the aforementioned sample and on $Ca_2CuO_2Cl_2$ (Na-CCOC) [62]. This allowed to reconstruct an image of the momentum structure of charge order.

Similar results [81] followed in highly underdoped Na-CCOC samples: here, charge modulations is revealed along the Cu-O bond direction, with a periodicity of 4 lattice unities. This occurrence demonstrated that this order was able to break the symmetry of all electronic states over an extended energy range. The charge order was associated to bond-centered, locally unidirectional domains persisting all the way up to the energy scales of the pseudogap regime.

From there a study on a mono-layered $Bi_{2y}Pb_ySr_{2-z}La_zCuO_{6+\sigma}$(Bi2201) [116] demonstrated that the charge order is compatible with instabilities arising from the antinodal regions of the Fermi surface. The same experiment, repeated on a Bi2212 sample [76], provided similar results: this occurrence sparked the idea of a connection between charge order and the pseudogap, since the two phenomena appeared to nucleate at comparable temperatures. This allowed to indisputably demonstrate a competitive behavior of charge order and superconductivity near the Fermi energy [99] and from there a number of similar studied gave further evidence of this phenomenon [60][86][48].

The next big step in the comprehension of the charge order phenomenon was achieved with the usage of hard and soft RIXS, since they were becoming increasingly less impractical alongside the increasing availability of synchrotron radiation sources. In 2002 a thin film of oxygen doped La_2CuO_4 at the O-K edge (1s $\rightarrow$ 2p, $\hbar\omega \simeq$ 530-550 eV) and $Cu - L_{3,2}$ edge (2p $\rightarrow$ 3d, $\hbar\omega \simeq$ 920-960 eV) was investigated, and it was revealed that during the resonant process a single hole excited up to 82 electronic charges [1].

This result is regarded as one of the key figures of merit for resonant x-ray methods, and represents the foundation mechanism underlying the success of RXS in detecting weak ordering phenomena (such as charge order) in the cuprates [34].

This knowledge confirmed RXS as a test capable of uncovering a number of otherwise hidden phenomena, and rapidly led to the discovery of a periodic electronic density modulation in a $Sr_{14}Cu_{24}O_{41}$ sample [2]. It is worth mentioning that the signal disappears if the incident photons are detuned, with respect to the resonant edge, even just by few eV,

After this discovery, a study on $La_{1.875}Ba_{0.125}CuO_4$ [4] allowed to confirm not only the presence of charge order, but also that this order manly affects the electronic cloud, distorting vice-versa only secondarily the lattice. Furthermore, the narrow dependence that the found peak had with respect to the out-of-plane momentum allowed to establish this charge order as nearly 2 dimensional (figure 4.1).

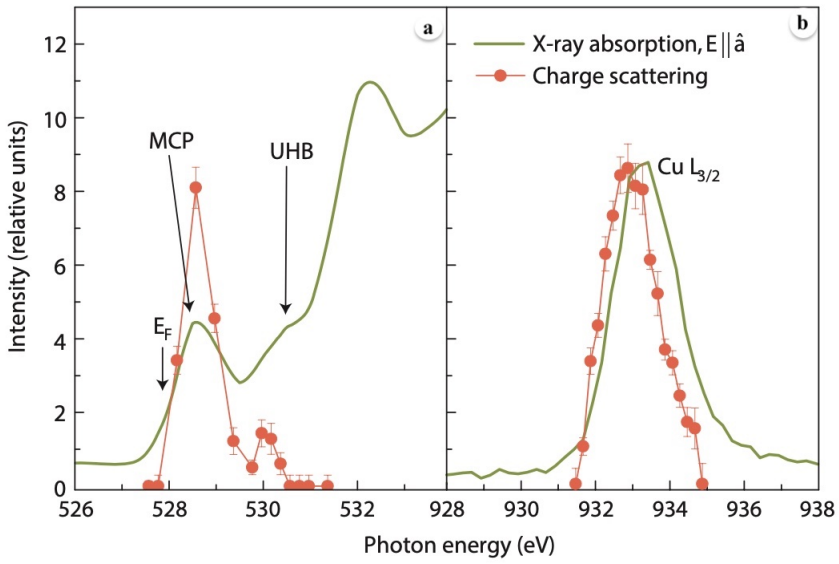

Figure 4.1: Resonant soft x-ray measurements of the charge order peak at the O-K (a) and CuL_3 (b) with highlighted excitation in the mobile carrier peak and upper Hubbard band [4]

After these pioneering experiments, the literature concerning the presence of charge order is cuprates underwent a flourishing decade, with RXS central in the field, and crucial to discover charge order in many other curate families.

4.2 Charge order in YBCO

Among the cuprates where a clear evidence of charge order was still missing, YBCO was the most important compound.

Finally, in 2007 a sample of $YBa_2Cu_3O_{6.51}$ at extremely low temperatures (1.5 K) and extremely high magnetic fields (62 T) showed what was descibed as "a reconstruction of the Fermi surface caused by the onset of a density-wave phase, as is thought to occur in the electron-doped copper oxides near the onset of antiferromagnetic order [34]"

And a nuclear magnetic resonance (NMR) on a similar specimen under comparable boundary conditions confirmed that it was due to charge order and that it was in competition with superconductivity here as well [119].

This observed competition suggested that charge order couldn't be observed alongside superconductivity. However, in 2012 such hyphotesis was proved to be wrong in the RIXS work by Ghiringhelli et al.. Here, the first directed observation of charge order at zero magnetic field was obtained. RIXS spectra were measured varying the planar projection of the momentum in the H0 direction of the reciprocal space (figure 4.2).

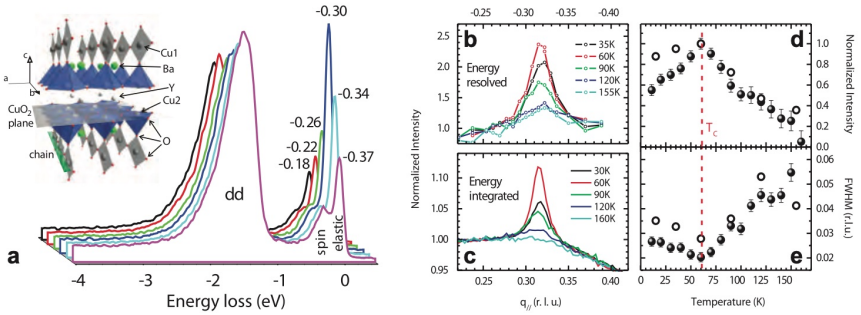

Figure 4.2: Energy loss scans (a) of momentum dependence (H0 direction) for a $(Nd, Y)Ba_2Cu_3O_{6+x}$ specimen, energy resolved (b) and energy integrated (c) momentum dependence, energy dependence of the peak intensity (d) and full-width-at-half-maximum (e) [50]

The quasi elastic intensity of the spectra, i.e. at energy losses close to 0, changes by changing by momentum, with a clear maximum at ~ 0.31 r.l.u. The peak, which is determining by integrating the quasi-elastic intensity vs q, is a signature of a periodic charge modulation.

This paper showed the crucial role RIXS could have had in the study of charge order in the cuprate CuO_2 layers. Many works therefore followed, trying to elucidate the properties of CDW and the role of these charge

modulations in the physics of the cuprates [16] [18] [64].

All these RIXS studies disclosed the strong difference between the charge ordering previously observed under high magnetic fields,and this novel one measured without field.

4.3 Universality of charge order among cuprates

CDW in absence of magnetic field were discovered using RXS in other compounds, as Bi2201 [33] and Bi2212 [99]. In particular, a comparison between the RXS results and the Fermi surface measured using angle-resolved photo emission spectroscopy (ARPES) in Bi2201 [33] allowed to calculate a quantitative connection between the mentioned values of wavevectors and the momentum vector connecting the tips of the Fermi arcs. This occurrence suggested a possible link between charge order and low-energy electronic structure [34].

Finally, CDW were discovered in Hg-based cuprates. $HgBa_2CuO_{4+\sigma}$ (Hg1201), possessing a tetragonal unit cell, was characterised by the highest structural symmetry of the family. The first evidence of charge order arrived from measurements of the Hall and Seebeck coefficients in underdoped Hg1201 and quantum oscillation, and the first peak of charge order appeared thanks to RIXS at $p \simeq 0.09$ and T=72K [101].

The exceptionally high T_C of this compound, together with the short correlation of the charge order, confirmed an anti-correlation between charge order and superconductivity, in common with all the other cuprate families.

Having closed the circle on cuprate compounds, a first, comprehensive of all charge order phenomena, was redacted for the doping dependence of the onset temperature (figure 4.3a) and the correspondent wavevectors (figure 4.3b).

In the first figure one can clearly see that the maximum of the CDW occurs in all the different compounds at a doping level, around 12%, corresponding to the depression of the superconducting dome in the underdoped regime.

The onset temperature changes inversely in respect to the variation of the charge order amplitudes and correlation lengths while an higher amplitude performs better at suppressing superconductivity.

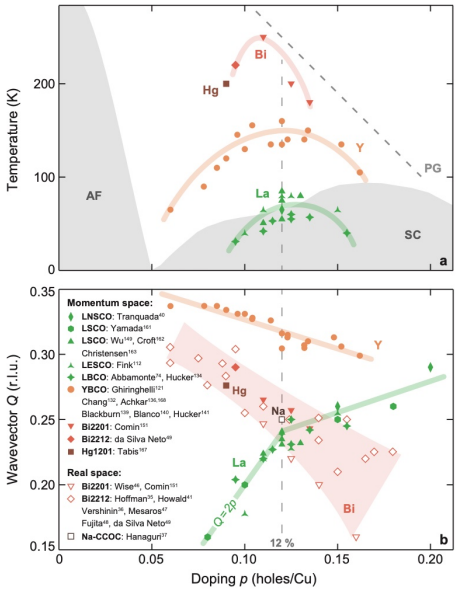

Figure 4.3: Onset temperature of charge order vs hole doping (a) and doping dependence of charge order wavevectors [104][120](b), full symbols are from momentum-resolved probes (RXS, XRD, neutron scattering), while open symbols are from real-space methods (STM). Colored lines are guides-to-the-eye; the vertical dashed line marks the location of the doping p=0.12 [34]

The second figure clearly shows two differences between CDW and the stripes in the La-based compounds [34]:

- In the latter ones, both charge order and incommensurate antiferromagnetic spin order coexists, whereas they cancel each other out elsewhere.
- La-based cuprates have an evolution of the charge order wavevector that has an opposite sign with respect to non La-based cuprates, phenomena possibly related to a nesting scenario.

These two occurrences highlight that, while a common charge ordering behavior is present across all cuprates, a clear difference has to be made between stripe order "stabilized by soft tilt distortions of the oxygen octahedra surrounding the Cu ions in this lattice structure" [47] and CDW.

4.4 Possible connection with the pseudogap

CDW is present in the region of the phase diagram, that sets on below T^*. This region, as previously introduced, is called the pseudogap region.

The origin and characteristic of the pseudogap are far from clear, but some guesses have been advanced on the basis of the information the researches had and have obtained over time. First and foremost on its origins they've been attributed to one of either motives [47]:

- A crossover due to electronic correlations, that also generate antiferromagnetic short-range order

- A phase transition with a broken symmetry that is 'hidden' to most experimental probes

The charge order was ruled out as a determining factor of the pseudogap, since the two phenomena show different temperature vs doping dependencies. The opposite case (i.e. pseudogap determining CDW) is still under consideration, since the possible dependence of the pseudogap on strong correlations could make it a precursor of the charge order.

Against this hypothesis a study on overdoped $(Bi, Pb)_{2.12}Sr_{1.88}CuO_{6+}$, where electronic correlation are weakened, found a charge order correlation length that follow the accepted behaviour, decreasing along an increase in temperature, but shows an onset temperature higher than room temperature, hence well above the T^* of the pseudogap [50].

4.5 An additional charge order peak

A recent RIXS study by Arpaia and Ghiringhelli [9], focusing on the temperature evolution of the charge order peak, gave some new insights on the nature of charge order and on its different components.

Here, RIXS spectra were taken at numerous temperatures (from 20 K to 270K in several intervals) on both $YBa_2Cu_3O_{7-\delta}$ and $Nd_{1+x}Ba_{2-x}Cu_3O_{7-\delta}$ thin films, spacing in doping from the AF region, up to the slightly overdoped region [11, 14, 13]. Measurements were taken at the Cu L3 edge (∼930 eV), over a broad in-plane wave vector ranges (q || = 0.17 to 0.46 reciprocal lattice units, r.l.u.).

The data show the presence of a peak along q || = (H, 0) (near-zero energy loss) at any temperature under investigation (figure 4.4). To get the peak, the RIXS

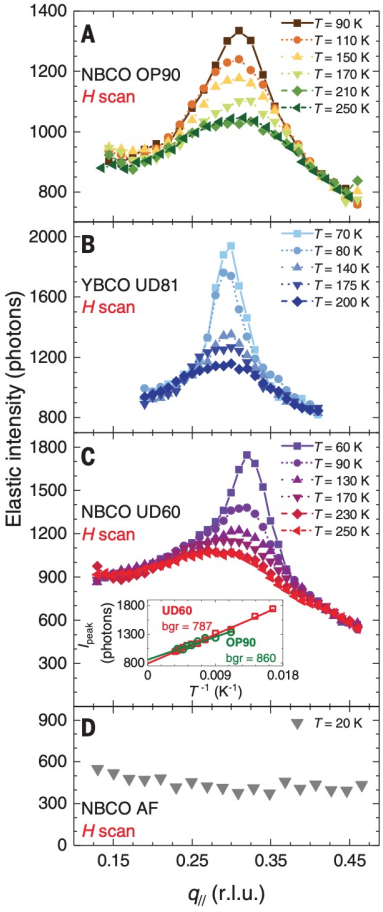

Figure 4.4: Quasi-elastic scan along the (H, 0) direction for several $YBa_2Cu_3O_{7-d}$ and $Nd_{1+x}Ba_{2-x}Cu_3O_{7-d}$ films with different oxygen dopings [9]

spectra are integrated in the energy interval [–0.2 eV, +0.15 eV]. The background is removed using the integrated quasi-elastic intensity of the spectra measured in the (H,H) direction, where the charge order peak is absent.

At high temperatures, the peak is influenced by a single broad Lorentzian peak (the broad peak, BP); at lower temperatures, a narrow peak appears in addition to the first (the narrow peak NP) (figure 4.5).

In this work the authors show that the broad peak, dominant at high temperature, is fluctuating in nature, i.e. it is characterized by finite energies in the meV range; the narrow peak is instead nearly static, and it represents the quasi critical, already known, CDW, appearing only below an onset temperature T_{QC} lower than the pseudogap temperature.

The main discovery of the experiment is the ubiquitous presence (both in temperature and doping) of a broad peak caused by dynamical charge density fluctuations, which don't compete, or compete only mildly, with superconductivity, and are present at temperatures much higher than the pseudogap [9].

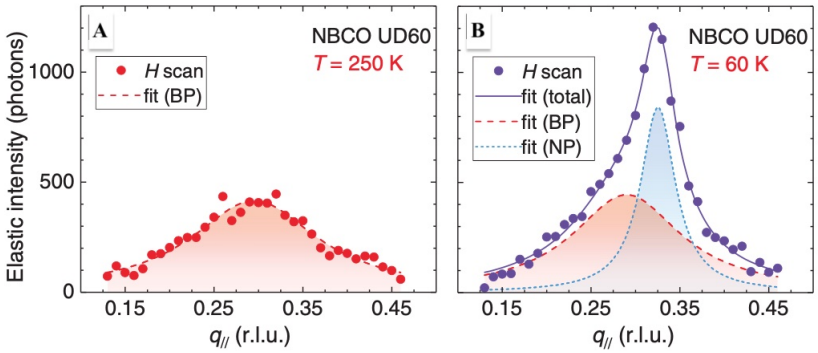

Figure 4.5: High temperature peak and NP and BP decomposition at 60 K [9]

After this first discovery, several studies have been performed by RIXS in the last two years on different families of cuprates, exploring the temperature and doping dependence of the charge order phenomenon in its whole. The common result is that very short ranged charge density modulations are present at any investigated temperature and in a broad doping range [10]. They survive at temperatures above not only the onset of CDW, but also the pseudogap temperature. The T-p phase diagram, shown in the previous chapters, is strongly modified: the presence of these pervasive high temperature charge fluctuations might have a decisive role to understand the different orders and regions populating the phase diagram. Based on these experimental results, several proposals, linking these fluctuations either to

the superconducting pairing mechanism or to the strange metal phase, have already been formulated.

Is has been hypothesised that the CDW and the CDF can develop differently in different region of the phase diagram where the NP could develop at the expenses of the BP. Is possible that CDFs are born alongside CDWs but weren't able to achieve criticality and thus establish long-range correlations.

This is the possibly the reason why CDFs account for the strange metal behavior. In fact, the narrow behavior of CDW give rise to anisotropic scattering dominated by the hot spots on the Fermi surface. CDFs, instead, characterised by a correlation length of 1-2 wavelenghts, affect all states on the Fermi surface nearly equally, resulting in an essentially isotropic scattering rate. [98]

In addition to this their characteristically low energy (tens of meV) would allow them to produce a linear scattering rate all the way to 100-120 K.

These results shadow the next steps for the researches on the topic. The effect of magnetic field on CDF could account for the Planckian transport that destroys superconductivity.

Furthermore the possible bridge among CDW and CDF could mean the presence of CDW at very low energy as well.

To test for either of these possibility it in necessary to be able to find collective modes at energy in lower than 1 meV and check for their correlation length. But no machinery is able to achieve such a precise test at the moment.

Chapter 5

Charge density fluctuations: determination of their energy from the RIXS spectra

5.1 Foundation of the analyses

Each discovery relies on the ability to think of an experiment that could extract relevant information from a spectra. The information then have to be processed in order to read what's behind them in a way that allows to compare this new data with the ones of previous studies.

The work of this thesis starts from the raw data of the experiment highlighted at the end of the previous chapter [9]. In addition to what has been done in that work, the aim here is to extract the energy value of the CDFs.

A direct measurement of the energy would require the determination of the feature representing the CDFs in the RIXS spectra. Since the energy of the CDFs is theoretically expected to be in the range of few tens meV, the CDF peak cannot be resolved from the pure elastic component at zero energy loss and to the several phononic branches which are present in the range between few meV up to about 100 meV: this occurrence is of course related to the energy resolution of the RIXS spectra, which is in the range of 60 meV.

An alternative path has to be chosen, in order to determine the CDF energy. The solution is given by the temperature dependence of the RIXS spectra in the quasi elastic region. Indeed, the CDFs are a collective excitation phenomenon, obeying to the Bose-Einstein statistics. As a consequence of that, the temperature dependence of the intensity of the quasi-elastic region of the RIXS spectra is connected by the CDF energy value. Indeed

the pure elastic peak, mainly related to the scattering from the surface, is temperature independent.

So, the aim is to integrate the quasi-elastic region of the RIXS spectra. From the value of this integral, measured at a fixed momentum as a function of the temperature, the energy of CDF can be extracted fitting the data with a Bose type equation.

However, before proceeding to this integration, a very careful analysis has to be performed. Indeed, in Ref. [9] the spectra have been integrated in the range between 100 meV and -150 meV, including therefore all the phonon contributions. Here, in order to carefully determine the CDF energy, we want to minimize the phonon contribution, which is also temperature dependent. The interval of integration has to be squeezed down to [24, -100] meV, which is very detrimental for the signal to noise ratio.

Before doing the fit of the data with the Bose-type equation, the spectra have to be aligned with a level of precision higher than what was needed in Ref. [9]. Since the resolution of the spectra is 60 meV, an "alignment strategy", including different "moves", has to be thought.

This thesis work, on which this chapter is based, mainly concerned 1) the realization and achievement of a fine alignment procedure of the RIXS spectra; 2) their integration in a range comparable with the energy resolution of the spectra; 3) the fit of the integrals measured vs temperature with a Bose equation; 4) the determination of the CDF from the fit.

Realizing this work for two different NBCO samples having different doping (optimally-doped and under-doped), I have been able to extract not only the CDF energy, but also to determine their energy dependence.

5.2 Data selection and range of focus

In Ref. [9], the RIXS spectra have been measured in the momentum range between 0.15 and 0.45 rlu. This was done in order to study the temperature evolution of the quasi- static CDW peak and of the dynamical CDF peak. As discussed in the previous chapters, the CDW is strongly T-dependent, with an intensity which is maximum at the critical temperature T_C, and decreasing both below T_C (being the superconductivity a competing order) and above T_C, disappearing at an onset temperature which is below the pseudogap. Such a strong T-dependence, which is on top the temperature dependence of the CDF, can affect the object of our analysis and the Bose fit we want to perform, negatively affecting the energy value we want to extract. Luckily, the CDW peak is narrow (being characterized by a rather long correlation length), and its contribution can be easily neglected going

to q values far from q_{CDW}. For our analysis we have therefore considered to investigate the tails of the CDF peak, where CDWs are absent, focusing on the ranges q≤0.22 ⋃ q≥0.40.

The analyses was carried out using the software Origin, that offers a wide number of tools to handle the considerable amount of data under analyses.

First step of the analysis work required the normalization of the spectra. This is needed to properly compare spectra acquired at different temperatures, in a rather long range of time. The synchrotron flux is indeed time-dependent, and this affects of course also the output signal, i.e. the intensity of the RIXS spectra, to whose changes we want to attribute a meaning.

The normalization of all the spectra was done using the area of the dd excitations, which we know has to be temperature independent [51].

After that normalization, we have interpolated with Origin all the spectra on the same x (energy loss) axis.

After that, the data were ready to be compared. As evident from figure 5.1, the data, as presented in Ref. [9], cannot be suitable for our new investigation. As evident in particular in the zoomed view of panel b, the spectra are strongly misaligned and cannot be integrated in a narrow range in the present form.

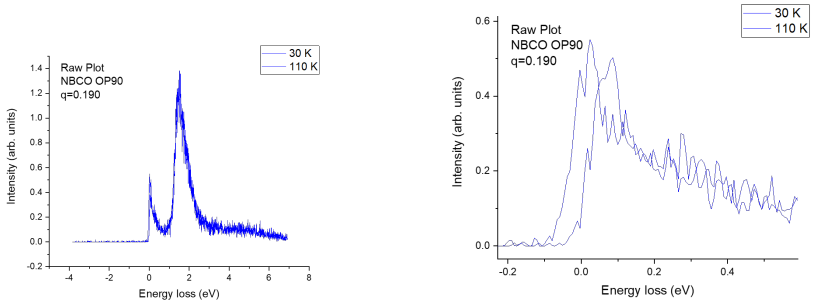

(a) Overview of the spectra

(b) Zoom of panel a, showing the quasi-elastic region of the spectra

Figure 5.1: RIXS spectra measured at q=0.19 r.l.u. as a function of the temperature, for the optimally doped sample OP90

5.3 Smoothing of the data and steps of alignment

Approaching now the plots, one by one to alignment them, it appeared clear that the noise was such that the probability to create an error, minimal as it could be for each step, was quite high in overall. Since that would cause

a cascade effect such to render the alignment itself moot, a direct only approach would not be possible.

In order to make the alignment easier and more precise the curves were smoothed using a 9 point average function offered by the program that made the curves much easier to follow and compare (figure 5.2).

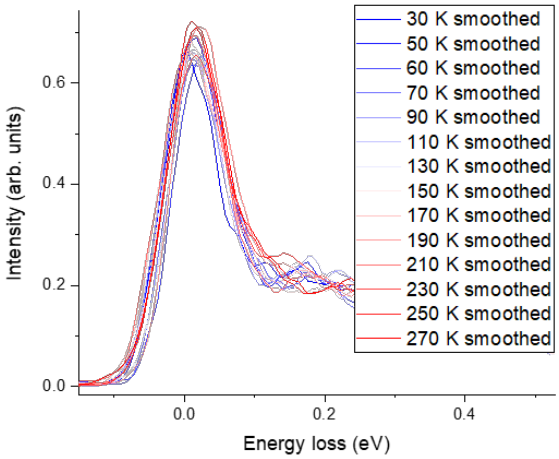

Figure 5.2: Energy loss plot of NBCO UD60, $q_{||}$ =0.19 for all temperature tested, smoothed using a 9 pts AAv algorithm

From this plot an alignment is possible but still susceptible to imperfection, the reason behind it is that, while the curves are focus of the right point and smoothed they remain different in height. This tend to change the shape of the rising edge making it hard to compare points that evolve following a different increment. In order to fix this all the curves were rescaled to the same height, chosen to be the one of the 30 K function for simplicity, dividing all the values related to the y axis by a factor equal to the ratio of the highest point of the given function and the highest point of the reference one (figure 5.3).

Subsequently, each function was aligned making use of a horizontal shift, keeping only the 30 K in position. The alignment was performed among curves close in temperature, but taking into consideration the shape of each one as well. The alignment was performed zooming in on relevant details of each temperature function and aligning using those as visual reference, at this stage the attention was solely focused on the left rising edge and the peak and little consideration was lend to the phonon breathing region following on the right.

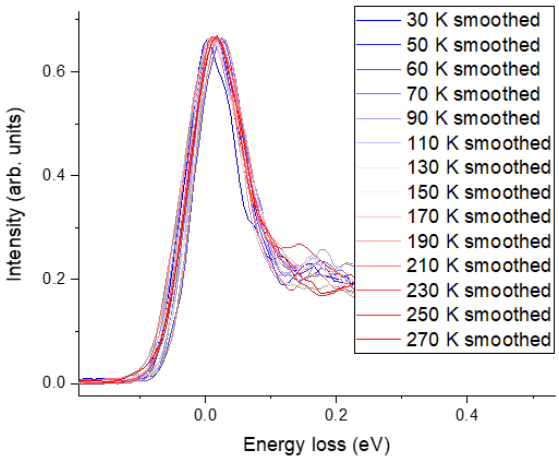

Figure 5.3: Energy loss plot of NBCO UD60, $q_{||}$ =0.19 for all temperature tested, smoothed using a 9 pts AAv algorithm and re-scaled to match each other's heights

The results were promising (figure 5.4) but, although some temperature appeared to match perfectly, some others didn't quite work out the way that was intended.

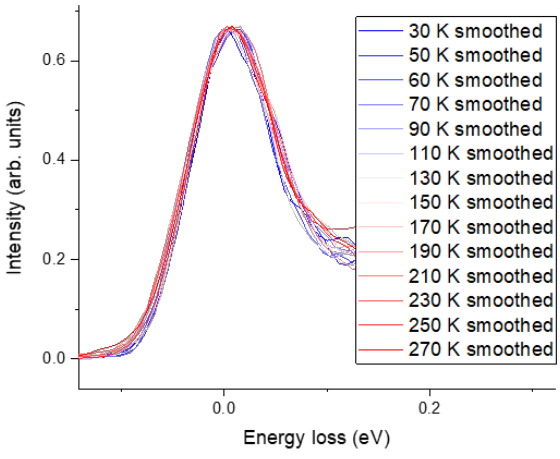

Figure 5.4: Energy loss plot of NBCO UD60, $q_{||}$ =0.19 for all temperature tested, smoothed using a 9 pts AAv algorithm and re-scaled to match each other's heights, aligned on visual reference

Before scaling back to their original height further steps were needed.

In order to improve on the previous results, all the curves that weren't satisfactory were reworked, this time moving the attention on a different feature. Making use of a pre-written algorithm the first and second derivative of each chosen function were calculated and plotted together, then orderly underwent all the passages previously described to be again aligned under the best possible condition (figure 5.5). The noise present in the derivative, and the second in particular, was such that improvements were possible only moving from pre-aligned data that only needed minor adjustments.

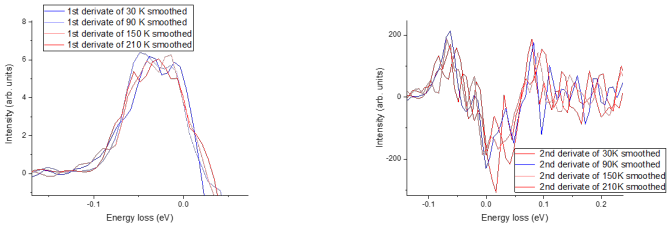

(a) First derivative (b) Second derivative

Figure 5.5: First and second derivative of the energy loss plot of NBCO UD60, $q_{||}$ =0.19 for some of the temperature tested

This further procedure allowed to fix some of the imperfection that were found before, but some other were such that no good comparison could be made or the adjustments performed with two different procedure seemed in opposition. To find the right placement for these functions the dd excitation region of the spectra was brought forth in focus.

The reason why this was done is that the dd excitations aren't much influenced by temperature having as such a spectra that remains mostly invariant among one function and the other. Even tough looking for spikes or derivative in this region didn't show much promise, the smoothed profile was still useful via its local position as a tell suggesting possible adjustment that the region of interest (-150 to +100 meV) might not have shown to the eye. This was done in some cases for both the NBCO OP90 and NBCO UD60 (figure 5.6) to various degree of success.

At this point most data were properly aligned, for the few that couldn't be placed with confidence I had to think of a new approach. Since the problem was the noise cause by the marginal experimental resolution I thought to decompose the peak that's influenced by charge order. Origin in fact offers a tool for peak fitting that makes use of a decomposition reconstructing the peak as a superimposition of Gaussian functions (figure 5.7). This decomposition allowed to isolate the noise in sharp and less intense curves

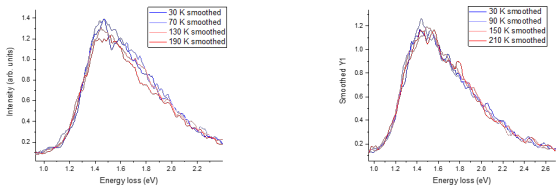

(a) NBCO UD60 (b) NBCO OP90

Figure 5.6: Focus on the smoothed dd excitation of the energy loss plot of NBCO, $q_{||}$ =0.19 for some of the temperature tested

subtracted from the overall picture giving back a clear profile for the components that gives to the plot the attributes reflecting the physical properties of the material.

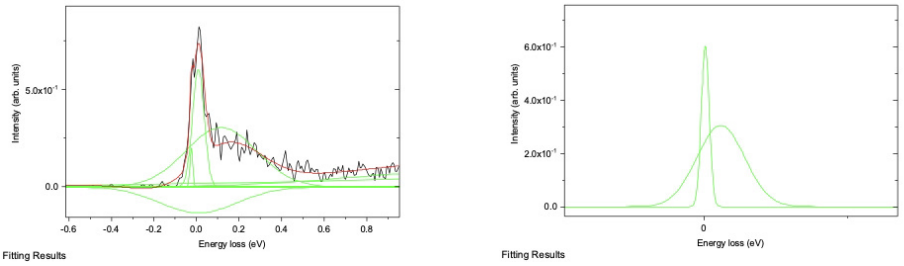

(a) Original peak in black, Gaussian functions obtained by decomposition in green, sum of these function in red

(b) Selection of the most influential Gaussian functions

Figure 5.7: Peak fitting of the energy loss plot of NBCO, $q_{||}$ =0.19, decomposition performed diving the peak in a series of Gaussian function that superimposed restore the peak while clearing the noise

In this way the alignment could be checked by subtracting the noise and looking at what appears to be a not tampered component of the peak. Doing this for both the temperatures under analyses allows to clearly see what incongruities remained after the previous steps. For example I present the case of two functions among the several I had to work with, here (figure 5.8)

I made use of the described procedure to perform the final adjustments at the position of the 90K function with respect to the 30K one, seeing that the former was still a little bit falling right; the difference among the two is really minimal, confirming the effectiveness of the previous steps, and the similarity among the decomposed component of the two set of data confirms the usefulness of this last used tool.

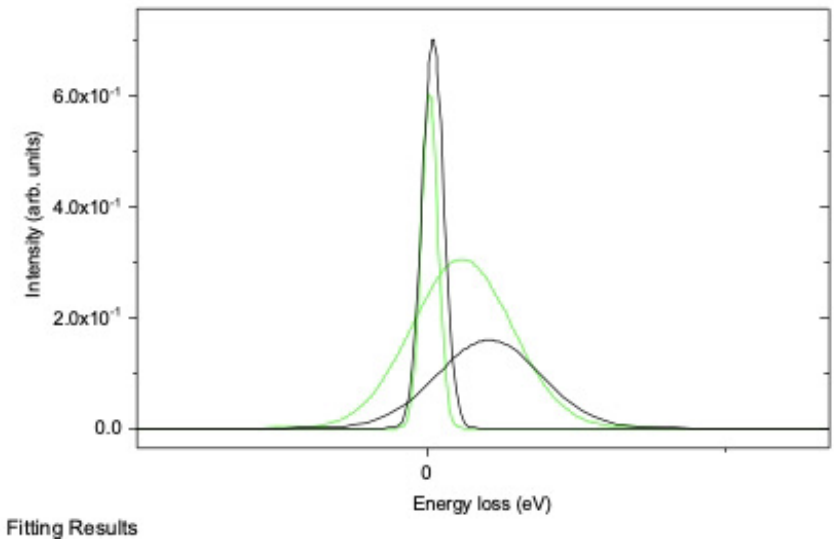

Figure 5.8: Peak fitting of the energy loss plot of NBCO, $q_{||}$ =0.19, decomposed in Gaussians for the 90K (in black) and 30K (in green) functions

5.4 Results of the alignment

As an example of the successful process presented in the previous section, I show for a fixed q the the RIXS spectra aligned at all temperatures for both the sample NBCO OP90 and NBCO UD60 (figure 5.9). The difference, with respect to the spectra presented before the fine alignment procedure, is evident

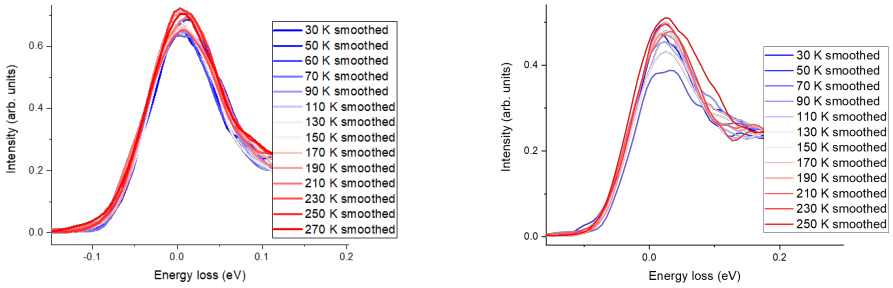

(a) NBCO UD 60

(b) NBCO OP 90

Figure 5.9: Energy loss plot, $q_{||}$ =0.19 for all temperature tested, after the process of alignment

Once the spectra are aligned, I calculated the integral in the region between -100 meV and +24 meV. As previously mentioned, the range has

been chosen to minimize the phonon contribution.

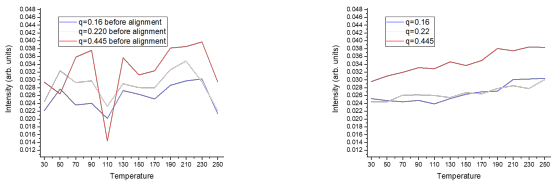

(a) Before alignment (b) After alignment

Figure 5.10: Integrated energy loss plot of NBCO OP90, $q_{||}$ =0.19, from -100 meV to +24 meV for some of the temperatures tested, showcased with the same data before alignment

In figures 5.10 and 5.11 I show the same curves, with the integral of the quasi elastic region of the RIXS spectra vs temperature, before and after the alignment. The behavior after the alignment is much smoother and the temperature dependence much clearer: the Bose fit can therefore be performed.

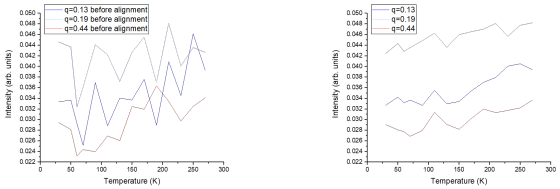

(a) Before alignment (b) After alignment

Figure 5.11: Integrated energy loss plot of NBCO UD60, q ||=0.19, from -100 meV to +24 meV for some of the temperatures tested, showcased with the same data before alignment

For the fit, I have used the following equation:

$$I = A + B * (1 + \frac{1}{exp(E/(k_B * T)) - 1})$$

In this model A is an additive parameter, temperature independent and q dependent, which reflects the presence of the pure elastic signal in the integral under investigation. B is a multiplicative parameter, both temperature and q independent, related to the intensity of the CDF at zero temperature. Finally E is the Bose energy, related to the CDFs.

In figure 5.12 I have presented the the experimental curves together with the Bose fit I have performed for each q value.

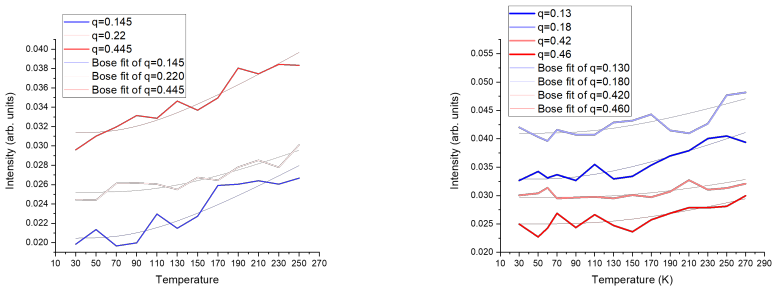

(a) NBCO OP90 (b) NBCO UD60

Figure 5.12: Integrated energy loss plot of NBCO OP90 and NBCO UD60, $q_{||}$ =0.19, from -100 meV to +24 meV for some of the temperatures tested, overlapped with the respective Bose equations, iterated until convergence

The result of the fit, for what concerning the additive constant an the energy of the CDF, is presented in figures 5.13 and 5.14.

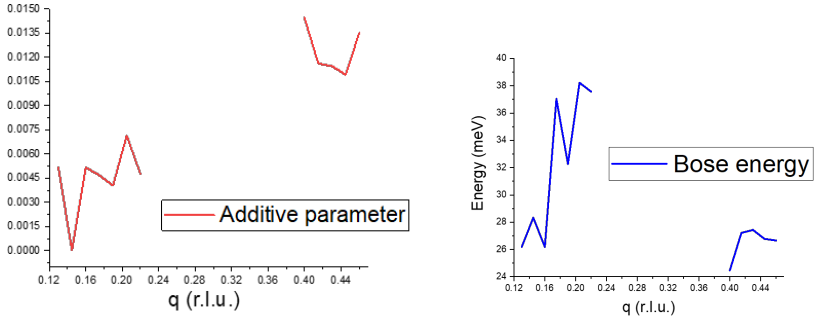

(a) Additive parameter (b) Bose energy

Figure 5.13: Bose parameters converged onto the integrated functions of NBCO OP90, $q_{||}$ =0.19, from -100 meV to +24 meV for all the temperatures tested

The fits tell us that the energies of the CDF are in the range of few tens of meV (20-40 meV), as expected by theory [98].

Furthermore, the evolution with doping suggests that this energy decrease as the doping level increase.

The final results were plotted in a 3D graph to offer a better overview of both the experimental curves with the integrals of the RIXS spectra and the theoretical curves used to fit the data (figures 5.15 to 5.18).

The aim of the project was mainly focused on obtaining a reliable process of alignment for an energy loss spectra with spacial dimensions competing with the experimental resolution of the spectrometer employed. Further-

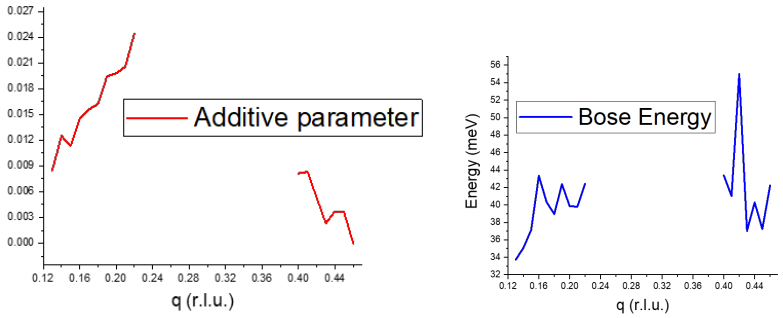

(a) Additive parameter (b) Bose energy

Figure 5.14: Bose parameters converged onto the integrated functions of NBCO UD60, $q_{||}$ =0.19, from -100 meV to +24 meV for all the temperatures tested

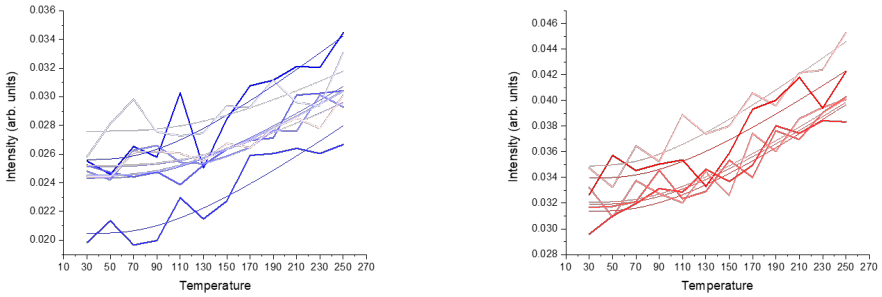

(a) Low wavevectors (b) High wavevectors

Figure 5.15: Energy loss plot of NBCO OP90, for all wavevectors and for all the temperatures tested, after the process of alignment

more there have been obtained results that describe the evolution of CDFs in the spectra and estimate their energy via a Bose distribution function. The integrated results shows that the CDFs, represented by their influence in producing the BP, appear across both all the tested wavevectors and more importantly at temperatures way higher than both the T_{QC} and T_C of the tested material. This is in no way a definitive calculation and further studies will have to follow in the field on several cuprates before CDFs characteristic can be precisely defined. But it is a worthy path to follow to clarify a phenomena influencing superconductivity across all the phase diagram. The way, as it was paved by several team composed by capable researchers, seems as promising as ever.

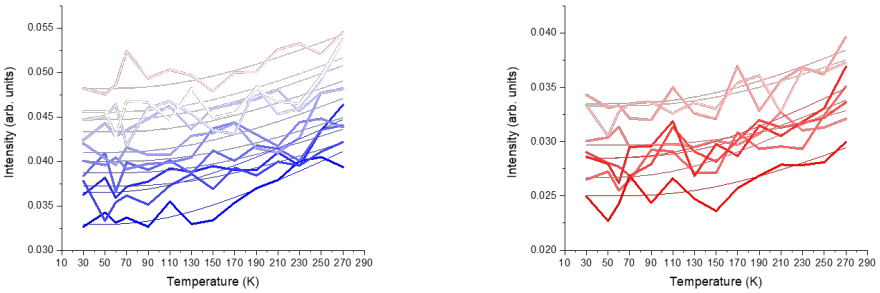

(a) Low wavevectors (b) High wavevectors

Figure 5.16: Energy loss plot of NBCO UD60, for all wavevectors and for all the temperatures tested, after the process of alignment

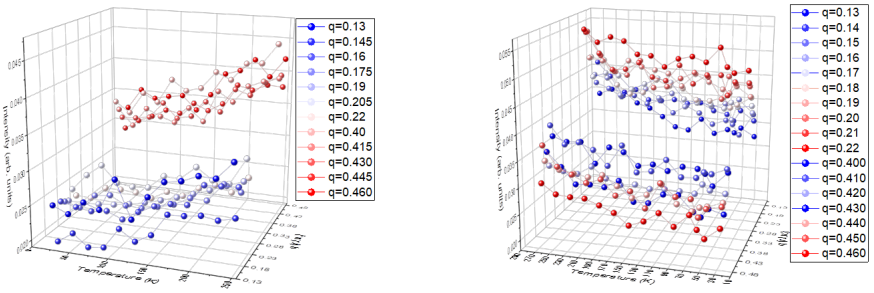

(a) NBCO OP90 (b) NBCO UD60

Figure 5.17: Integrated energy loss plot of NBCO OP90 and NBCO UD60 from -100 meV to +24 meV for all the wavevectors and the temperatures tested, after the process of alignment

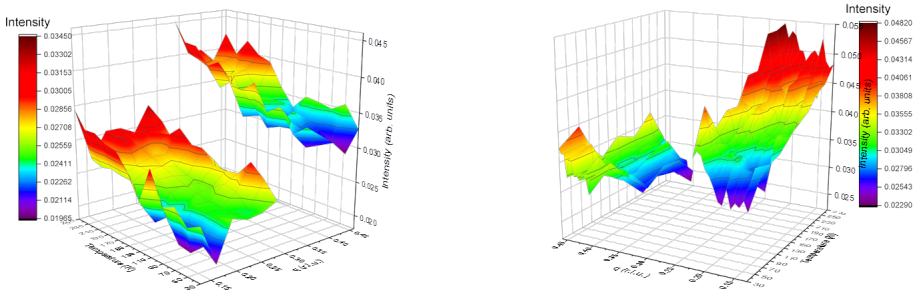

(a) NBCO OP90 (b) NBCO UD60

Figure 5.18: Integrated energy loss plot of NBCO OP90 and NBCO UD60 from -100 meV to +24 meV for all the wavevectors and the temperatures tested, after the process of alignment, surface reconstructed with chromatic scale following integrated intensity

Chapter 6

Conclusions

Since the early age of superconduction a century has passed during which the numerous researchers that took interest in the field had reached a much deeper understanding of what a superconductor is and what it is possible to make from it. If once only a handful of compounds were able, under the most extreme temperature condition achievable only in laboratories, to perform superconductivity, slowly but surely an ever increasing number of materials were found or alternatively engineered that not only showed the massive decrease in electrical resistivity representative of the phenomena, but could do so under much less extreme condition than their original counterparts.

These developments have lead to the concept of phase diagram of superconductivity where doping level of semiconductors and temperature interactions where mapped and subsequently studied to understand how either influenced the materials and how to possibly harness this newly found knowledge to create superconductors that could operate at, ideally, room temperature and pressure.

This feat hasn't been reached yet but the improvements are frequent and promising, recent studies takes advantage of the progress in the synthesis of thin films and hetero-structures to systematically manipulate the electron system in the cuprate by hetero-structures [47]. Cuprates are indeed a recursive name in the papers that concern superconductivity since they have been found to be, as previously discussed, a family capable of performing under no particular external condition up to 140 K, and consistently across several different compound of the family even tough at variable temperatures.

Cuprates are not necessarily the receipt for room temperature application, it is in fact worth mentioning the recent results reached with As-grown AgF_2 that has been theorised to reach superconductivity at up to 195 K [53], or alternatively another study report superconductivity in a photochemically

transformed carbonaceous sulfur hydride system up to 287.7 ± 1.2 K but only under 190 gigapascal of pressure [100]. Nonetheless what cuprate offers is a consistent framework blooming with phases that interact with each other in complex and exiting ways, rearranging the electronic properties of the structures in domains that competes with each other possibly still hiding new properties that could revolutionise the field once again.

Through years of studies scientists have discovered the phenomena of charge order and are now uncovering what governs it and how. Numerous theories have been proposed following experimental milestones or new theoretical propositions and the leading debate covers topic such as CDWs and CDFs. We couldn't be here if new probing techniques such as RXS hadn't been developed and models to read those data hadn't followed, and still old and new challenges remains that will require further studies.

What we know is that CDWs compete with superconductivity, this however is not necessarily true for CDFs where it might as well be the opposite. The researches so far, as it was dealt in chapter 4, have studied the behavior of CDFs both in conjunction with CDWs and on their own. It was discovered that CDFs could very well be the missing piece we were looking for the understanding of the strange metal behavior above T^*. This is deeply connected with their minimal correlation length alongside their small energy factor. Furthermore hypothesis on the nature of CDFs have delved into theorising that they might be CDWs that could not go critical. This would suggest that we are still missing some pieces of information on CDWs, possibly at energy almost as low as CDFs. The influence this collective phenomena have on the electronic properties of cuprate will most likely be the key element needed for the next step in our understanding of HTS. In particular CDFs, 'given their wide persistence in the phase diagram, will possible occupy a role of great interest in the near future alongside long-range entanglement generically associated with quantum criticality [47]. The final passages of this paper had cleared, through the process of alignment, the energetic evolution of CDFs in two differently doped NBCO samples via a novel approach that account for the impossibility of a direct extraction of the results. The results coincide with the current theoretical trends both in energy levels and doping dependence against temperature. This demonstrate the effectiveness of the models used [98] and gives background data for future analyses.

Furthermore it might aid in speeding up the coming of these analyses. In fact, the bottleneck right now is caused by the inability of the scientific community to obtain a clear picture of these phenomena with an energy resolution high enough to clear the fog on their properties and relationship.

The technological improvements will surely lead to an improvements in the capability of the facilities in the coming years, and possibly the work of this thesis will aid in speeding up the process providing a ground to build on to create a repeatable process capable of getting around the problem of insufficient resolution. Alternatively, an entirely new approach will have to be created in order to do so; either way this is and will be a field that mustn't be underestimated since it could change the way the world itself functions.

Once people had to move the water from the rivers in buckets to irrigate the field, at that time the invention of what is now known as the Archimede's screw powered by a windmill was revolutionary; from then the world has changed dramatically, now people can harness electricity at the flick of a finger and fly across the oceans in hours. We live in an era of wonders where new invention are an everyday occurrence, but in this ever evolving world few things can really create a new revolution; we approach the idea of living on other planets and fathom the possibility of exploring the galaxy, we interface for the first time with artificial intelligence and find day after day new application of them in several field, we harness energy both from environmental sources and from atomic fission while waiting for the day of nuclear fusion, and we are now closer than ever to obtain a microscopic understanding of superconductivity towards realistic and affordable room temperature application. We will have to wait a little bit of time before some of these futures will became reality, others aren't so far, all are getting closer through the tireless work of generations of scientists that believe in a better future.... and who knows, maybe one day energy will be free, but that's a topic for another day.

Bibliography

[1] P. Abbamonte. "A Structural Probe of the Doped Holes in Cuprate Superconductors". In: *Science* 297.5581 (July 2002), pp. 581–584. DOI: 10.1126/science.1070903. URL: https://doi.org/10.1126/science.1070903.

[2] P. Abbamonte et al. "Crystallization of charge holes in the spin ladder of Sr14Cu24O41". In: *Nature* 431.7012 (Oct. 2004), pp. 1078–1081. DOI: 10.1038/nature02925. URL: https://doi.org/10.1038/nature02925.

[3] P. Abbamonte et al. "Resonant Inelastic X-Ray Scattering from Valence Excitations in Insulating Copper Oxides". In: *Phys. Rev. Lett.* 83 (4 July 1999), pp. 860–863. DOI: 10.1103/PhysRevLett.83.860. URL: https://link.aps.org/doi/10.1103/PhysRevLett.83.860.

[4] P. Abbamonte et al. "Spatially modulated 'Mottness' in La2-xBaxCuO4". In: *Nature Physics* 1.3 (Dec. 2005), pp. 155–158. DOI: 10.1038/nphys178. URL: https://doi.org/10.1038/nphys178.

[5] Luuk J. P. Ament et al. "Resonant inelastic x-ray scattering studies of elementary excitations". In: *Reviews of Modern Physics* 83.2 (June 2011), pp. 705–767. DOI: 10.1103/revmodphys.83.705. URL: https://doi.org/10.1103/revmodphys.83.705.

[6] Luuk J. P. Ament et al. "Resonant inelastic x-ray scattering studies of elementary excitations". In: *Rev. Mod. Phys.* 83 (2 June 2011), pp. 705–767. DOI: 10.1103/RevModPhys.83.705. URL: https://link.aps.org/doi/10.1103/RevModPhys.83.705.

[7] A. Amorese et al. "Enhanced spatial resolution of commercial soft X-ray CCD detectors by single-photon centroid reconstruction". In: *Nuclear Instruments and Methods in Physics Research Section A: Accelerators, Spectrometers, Detectors and Associated Equipment* 935 (Aug. 2019), pp. 222–226. DOI: 10.1016/j.nima.2019.03.010. URL: https://doi.org/10.1016/j.nima.2019.03.010.

[8] Masatoshi Arai et al. “Incommensurate Spin Dynamics in High Temperature Superconductor of Optimally Doped YBa2Cu3O7”. In: (Jan. 2000).

[9] R Arpaia et al. “Dynamical charge density fluctuations pervading the phase diagram of a Cu-based high-Tc superconductor”. In: *Science* 365.6456 (2019), pp. 906–910.

[10] Riccardo Arpaia and Giacomo Ghiringhelli. “Charge order at high temperature in cuprate superconductors”. In: *arXiv preprint arXiv:2106.00731* (2021).

[11] Riccardo Arpaia et al. “Probing the phase diagram of cuprates with $YBa_2Cu_3O_{7-\delta}$ thin films and nanowires”. In: *Phys. Rev. Materials* 2.2 (2018), p. 024804.

[12] Riccardo Arpaia et al. “Transport properties of ultrathin $YBa_2Cu_3O_{7-\delta}$ nanowires: A route to single-photon detection”. In: *Phys. Rev. B* 96.6 (2017), p. 064525.

[13] Riccardo Arpaia et al. “Untwinned $YBa_2Cu_3O_{7-\delta}$ thin films on MgO substrates: A platform to study strain effects on the local orders in cuprates”. In: *Phys. Rev. Materials* 3.11 (2019), p. 114804.

[14] Reza Baghdadi et al. “Toward $YBa_2Cu_3O_{7-\delta}$ Nanoscale Structures for Hybrid Devices”. In: *IEEE Trans. Appl. Supercond.* 25.3 (2014), p. 1100104.

[15] J. G. Bednorz and K. A. Mller. “Possible highT c superconductivity in the Ba?La?Cu?O system”. In: *Zeitschrift fr Physik B Condensed Matter* 64.2 (June 1986), pp. 189–193. DOI: 10.1007/bf01303701. URL: https://doi.org/10.1007/bf01303701.

[16] David Benjamin et al. “Microscopic Theory of Resonant Soft-X-Ray Scattering in Materials with Charge Order: The Example of Charge Stripes in High-Temperature Cuprate Superconductors”. In: *Phys. Rev. Lett.* 110 (13 Mar. 2013), p. 137002. DOI: 10.1103/PhysRevLett.110.137002. URL: https://link.aps.org/doi/10.1103/PhysRevLett.110.137002.

[17] R. J. Birgeneau et al. “Static and dynamic spin fluctuations in superconducting $La_{2-x}Sr_xCuO_4$”. In: *Phys. Rev. B* 39 (4 Feb. 1989), pp. 2868–2871. DOI: 10.1103/PhysRevB.39.2868. URL: https://link.aps.org/doi/10.1103/PhysRevB.39.2868.

[18] S. Blanco-Canosa et al. "Resonant x-ray scattering study of charge-density wave correlations in $YBa_2Cu_3O_{6+x}$". In: *Phys. Rev. B* 90 (5 Aug. 2014), p. 054513. DOI: 10.1103/PhysRevB.90.054513. URL: https://link.aps.org/doi/10.1103/PhysRevB.90.054513.

[19] L. Braicovich et al. "Dispersion of Magnetic Excitations in the Cuprate La_2CuO_4 and $CaCuO_2$ Compounds Measured Using Resonant X-Ray Scattering". In: *Phys. Rev. Lett.* 102 (16 Apr. 2009), p. 167401. DOI: 10.1103/PhysRevLett.102.167401. URL: https://link.aps.org/doi/10.1103/PhysRevLett.102.167401.

[20] L. Braicovich et al. "Magnetic Excitations and Phase Separation in the Underdoped $La_{2-x}Sr_xCuO_4$ Superconductor Measured by Resonant Inelastic X-Ray Scattering". In: *Phys. Rev. Lett.* 104 (7 Feb. 2010), p. 077002. DOI: 10.1103/PhysRevLett.104.077002. URL: https://link.aps.org/doi/10.1103/PhysRevLett.104.077002.

[21] L. Braicovich et al. "Magnetic Excitations and Phase Separation in the Underdoped $La_{2-x}Sr_xCuO_4$ Superconductor Measured by Resonant Inelastic X-Ray Scattering". In: *Phys. Rev. Lett.* 104 (7 Feb. 2010), p. 077002. DOI: 10.1103/PhysRevLett.104.077002. URL: https://link.aps.org/doi/10.1103/PhysRevLett.104.077002.

[22] L. Braicovich et al. "Resonant inelastic x-ray scattering from magnetic systems with angular resolution and polarization analysis of the scattered beam: Results on metallic Co, Fe, and Co ferrite at the $L_{3,2}$ edges". In: *Phys. Rev. B* 75 (18 May 2007), p. 184408. DOI: 10.1103/PhysRevB.75.184408. URL: https://link.aps.org/doi/10.1103/PhysRevB.75.184408.

[23] L. Braicovich et al. "Spectroscopy of strongly correlated systems: Resonant x-ray scattering without energy resolution in the scattered beam". In: *Physical Review B* 75.7 (Feb. 2007). DOI: 10.1103/physrevb.75.073104. URL: https://doi.org/10.1103/physrevb.75.073104.

[24] L. Braicovich et al. "The simultaneous measurement of energy and linear polarization of the scattered radiation in resonant inelastic soft x-ray scattering". In: *Review of Scientific Instruments* 85.11 (Nov. 2014), p. 115104. DOI: 10.1063/1.4900959. URL: https://doi.org/10.1063/1.4900959.

[25] Lucio Braicovich and Giacomo Ghiringhelli. "High-resolution resonant inelastic soft X-ray scattering (RIXS) A new spectroscopy for

the study of charge, orbital, spin and lattice excitations in materials with strong electron correlation". In: 35 (Oct. 2019).

[26] Lucio Braicovich et al. "Determining the electron-phonon coupling in superconducting cuprates by resonant inelastic x-ray scattering: Methods and results on Nd1xBa2-xCu3O7-". In: *Physical Review Research* 2.2 (May 2020). DOI: 10.1103/physrevresearch.2.023231. URL: https://doi.org/10.1103/physrevresearch.2.023231.

[27] J. van den Brink and M. van Veenendaal. "Correlation functions measured by indirect resonant inelastic X-ray scattering". In: *Europhysics Letters (EPL)* 73.1 (Jan. 2006), pp. 121–127. DOI: 10.1209/epl/i2005-10366-9. URL: https://doi.org/10.1209/epl/i2005-10366-9.

[28] N.B. Brookes et al. "The beamline ID32 at the ESRF for soft X-ray high energy resolution resonant inelastic X-ray scattering and polarisation dependent X-ray absorption spectroscopy". In: *Nuclear Instruments and Methods in Physics Research Section A: Accelerators, Spectrometers, Detectors and Associated Equipment* 903 (Sept. 2018), pp. 175–192. DOI: 10.1016/j.nima.2018.07.001. URL: https://doi.org/10.1016/j.nima.2018.07.001.

[29] S. M. Butorin et al. "Resonant X-Ray Fluorescence Spectroscopy of Correlated Systems: A Probe of Charge-Transfer Excitations". In: *Phys. Rev. Lett.* 77 (3 July 1996), pp. 574–577. DOI: 10.1103/PhysRevLett.77.574. URL: https://link.aps.org/doi/10.1103/PhysRevLett.77.574.

[30] U. Chatterjee et al. "Electronic phase diagram of high-temperature copper oxide superconductors". In: *Proceedings of the National Academy of Sciences* 108.23 (May 2011), pp. 9346–9349. DOI: 10.1073/pnas.1101008108. URL: https://doi.org/10.1073/pnas.1101008108.

[31] Su-Di Chen et al. "Incoherent strange metal sharply bounded by a critical doping in Bi2212". In: *Science* 366.6469 (Nov. 2019), pp. 1099–1102. DOI: 10.1126/science.aaw8850. URL: https://doi.org/10.1126/science.aaw8850.

[32] T. R. Chien, Z. Z. Wang, and N. P. Ong. "Effect of Zn impurities on the normal-state Hall angle in single-crystal $YBa_2Cu_{3-x}Zn_xO_{7-\delta}$". In: *Phys. Rev. Lett.* 67 (15 Oct. 1991), pp. 2088–2091. DOI: 10.1103/PhysRevLett.67.2088. URL: https://link.aps.org/doi/10.1103/PhysRevLett.67.2088.

[33] R. Comin et al. "Charge Order Driven by Fermi-Arc Instability in Bi2Sr2-xLaxCuO6 ". In: *Science* 343.6169 (Dec. 2013), pp. 390–392. DOI: 10.1126/science.1242996. URL: https://doi.org/10.1126/science.1242996.

[34] Riccardo Comin and Andrea Damascelli. "Resonant X-Ray Scattering Studies of Charge Order in Cuprates". In: *Annual Review of Condensed Matter Physics* 7.1 (Mar. 2016), pp. 369–405. DOI: 10.1146/annurev-conmatphys-031115-011401. URL: https://doi.org/10.1146/annurev-conmatphys-031115-011401.

[35] Philippe Corboz, T. M. Rice, and Matthias Troyer. "Competing States in thet-JModel: Uniformd-Wave State versus Stripe State". In: *Physical Review Letters* 113.4 (July 2014). DOI: 10.1103/physrevlett.113.046402. URL: https://doi.org/10.1103/physrevlett.113.046402.

[36] CrystalMaker. *Structure Type 069: La2CuO4 (LBCO)*. 2013. URL: http://som.web.cmu.edu/structures/S069-LBCO.html (visited on 07/08/2013).

[37] Reznik D. "Giant Electron-Phonon Anomaly in Doped La2CuO4 and Other Cuprates". In: *Advances in Condensed Matter Physics* 2010 (Jan. 2010). DOI: 10.1155/2010/523549.

[38] M. P. M. Dean et al. "Persistence of magnetic excitations in La2-xSrxCuO4 from the undoped insulator to the heavily overdoped non-superconducting metal". In: *Nature Materials* 12.11 (Aug. 2013), pp. 1019–1023. DOI: 10.1038/nmat3723. URL: https://doi.org/10.1038/nmat3723.

[39] Luca Delacrétaz et al. "Bad Metals from Fluctuating Density Waves". In: *SciPost Phys.* 3.3 (2017), p. 025.

[40] H. Ding et al. "Spectroscopic evidence for a pseudogap in the normal state of underdoped high-Tc superconductors". In: *Nature* 382.6586 (July 1996), pp. 51–54. DOI: 10.1038/382051a0. URL: https://doi.org/10.1038/382051a0.

[41] L.-C. Duda et al. "Resonant Inelastic X-Ray Scattering at the Oxygen K Resonance of NiO: Nonlocal Charge Transfer and Double-Singlet Excitations". In: *Phys. Rev. Lett.* 96 (6 Feb. 2006), p. 067402. DOI: 10.1103/PhysRevLett.96.067402. URL: https://link.aps.org/doi/10.1103/PhysRevLett.96.067402.

[42] V.J. Emery and S.A. Kivelson. "Frustrated electronic phase separation and high-temperature superconductors". In: *Physica C: Superconductivity* 209.4 (May 1993), pp. 597–621. DOI: 10.1016/0921-4534(93)90581-a. URL: https://doi.org/10.1016/0921-4534(93)90581-a.

[43] H. Eskes, L. H. Tjeng, and G. A. Sawatzky. "Cluster-model calculation of the electronic structure of CuO: A model material for the high-T_c superconductors". In: *Phys. Rev. B* 41 (1 Jan. 1990), pp. 288–299. DOI: 10.1103/PhysRevB.41.288. URL: https://link.aps.org/doi/10.1103/PhysRevB.41.288.

[44] ESRF$_b eamline_s taff$. *ESRF beamline specifics*. 2021. URL: https://www.esrf.fr/home/UsersAndScience/Experiments/EMD/ID32/RIXS.html.

[45] Thomas Faulkner and Joseph Polchinski. "Semi-holographic Fermi liquids". In: *Journal of High Energy Physics* 2011.6 (June 2011). DOI: 10.1007/jhep06(2011)012. URL: https://doi.org/10.1007/jhep06(2011)012.

[46] Eduardo Fradkin, Steven A. Kivelson, and John M. Tranquada. "Colloquium: Theory of intertwined orders in high temperature superconductors". In: *Reviews of Modern Physics* 87.2 (May 2015), pp. 457–482. DOI: 10.1103/revmodphys.87.457. URL: https://doi.org/10.1103/revmodphys.87.457.

[47] Alex Frano et al. "Charge ordering in superconducting copper oxides". In: *Journal of Physics: Condensed Matter* 32.37 (June 2020), p. 374005. DOI: 10.1088/1361-648x/ab6140. URL: https://doi.org/10.1088/1361-648x/ab6140.

[48] K. Fujita et al. "Simultaneous Transitions in Cuprate Momentum-Space Topology and Electronic Symmetry Breaking". In: *Science* 344.6184 (May 2014), pp. 612–616. DOI: 10.1126/science.1248783. URL: https://doi.org/10.1126/science.1248783.

[49] Gerald Gabrielse and Hans Dehmelt. "Observation of inhibited spontaneous emission". In: *Phys. Rev. Lett.* 55 (1 July 1985), pp. 67–70. DOI: 10.1103/PhysRevLett.55.67. URL: https://link.aps.org/doi/10.1103/PhysRevLett.55.67.

[50] G. Ghiringhelli et al. "Long-Range Incommensurate Charge Fluctuations in (Y, Nd)Ba2Cu3O6x". In: *Science* 337.6096 (July 2012), pp. 821–825. DOI: 10.1126/science.1223532. URL: https://doi.org/10.1126/science.1223532.

[51] G. Ghiringhelli et al. "Low Energy Electronic Excitations in the Layered Cuprates Studied by Copper L_3 Resonant Inelastic X-Ray Scattering". In: *Phys. Rev. Lett.* 92 (11 Mar. 2004), p. 117406. DOI: 10.1103/PhysRevLett.92.117406. URL: https://link.aps.org/doi/10.1103/PhysRevLett.92.117406.

[52] F. M. F. de Groot, P. Kuiper, and G. A. Sawatzky. "Local spin-flip spectral distribution obtained by resonant x-ray Raman scattering". In: *Phys. Rev. B* 57 (23 June 1998), pp. 14584–14587. DOI: 10.1103/PhysRevB.57.14584. URL: https://link.aps.org/doi/10.1103/PhysRevB.57.14584.

[53] Adam Grzelak et al. "Epitaxial engineering of flat silver fluoride cuprate analogs". In: *Phys. Rev. Materials* 4 (8 Aug. 2020), p. 084405. DOI: 10.1103/PhysRevMaterials.4.084405. URL: https://link.aps.org/doi/10.1103/PhysRevMaterials.4.084405.

[54] M. Guarise et al. "Measurement of Magnetic Excitations in the Two-Dimensional Antiferromagnetic $Sr_2CuO_2Cl_2$ Insulator Using Resonant X-Ray Scattering: Evidence for Extended Interactions". In: *Phys. Rev. Lett.* 105 (15 Oct. 2010), p. 157006. DOI: 10.1103/PhysRevLett.105.157006. URL: https://link.aps.org/doi/10.1103/PhysRevLett.105.157006.

[55] J N Hancock, G Chabot-Couture, and M Greven. "Lattice coupling and Franck–Condon effects in K-edge resonant inelastic x-ray scattering". In: *New Journal of Physics* 12.3 (Mar. 2010), p. 033001. DOI: 10.1088/1367-2630/12/3/033001. URL: https://doi.org/10.1088/1367-2630/12/3/033001.

[56] Y. Harada et al. "Polarization dependence of soft-x-ray Raman scattering at the L edge of TiO_2". In: *Phys. Rev. B* 61 (19 May 2000), pp. 12854–12859. DOI: 10.1103/PhysRevB.61.12854. URL: https://link.aps.org/doi/10.1103/PhysRevB.61.12854.

[57] Yoshihisa Harada. "Resonant Inelastic X-ray Scattering (RIXS)". In: *Synchrotron Radiation News* 31.2 (Mar. 2018), pp. 2–2. DOI: 10.1080/08940886.2018.1435947. URL: https://doi.org/10.1080/08940886.2018.1435947.

[58] M. W. Haverkort. "Theory of Resonant Inelastic X-Ray Scattering by Collective Magnetic Excitations". In: *Physical Review Letters* 105.16 (Oct. 2010). DOI: 10.1103/physrevlett.105.167404. URL: https://doi.org/10.1103/physrevlett.105.167404.

[59] M. W. Haverkort et al. "Nonresonant Inelastic X-Ray Scattering Involving Excitonic Excitations: The Examples of NiO and CoO". In: *Phys. Rev. Lett.* 99 (25 Dec. 2007), p. 257401. DOI: 10.1103/PhysRevLett.99.257401. URL: https://link.aps.org/doi/10.1103/PhysRevLett.99.257401.

[60] Y. He et al. "Fermi Surface and Pseudogap Evolution in a Cuprate Superconductor". In: *Science* 344.6184 (May 2014), pp. 608–611. DOI: 10.1126/science.1248221. URL: https://doi.org/10.1126/science.1248221.

[61] J. P. Hill et al. "Resonant Inelastic X-Ray Scattering in Nd_2CuO_4". In: *Phys. Rev. Lett.* 80 (22 June 1998), pp. 4967–4970. DOI: 10.1103/PhysRevLett.80.4967. URL: https://link.aps.org/doi/10.1103/PhysRevLett.80.4967.

[62] J. E. Hoffman. "Imaging Quasiparticle Interference in Bi2Sr2CaCu2O8delta". In: *Science* 297.5584 (July 2002), pp. 1148–1151. DOI: 10.1126/science.1072640. URL: https://doi.org/10.1126/science.1072640.

[63] C. C. Homes et al. "Optical conductivity of c axis oriented $YBa_2Cu_3O_{6.70}$: Evidence for a pseudogap". In: *Phys. Rev. Lett.* 71 (10 Sept. 1993), pp. 1645–1648. DOI: 10.1103/PhysRevLett.71.1645. URL: https://link.aps.org/doi/10.1103/PhysRevLett.71.1645.

[64] M. Hücker et al. "Competing charge, spin, and superconducting orders in underdoped $YBa_2Cu_3O_y$". In: *Phys. Rev. B* 90 (5 Aug. 2014), p. 054514. DOI: 10.1103/PhysRevB.90.054514. URL: https://link.aps.org/doi/10.1103/PhysRevB.90.054514.

[65] S. Johnston et al. "Systematic study of electron-phonon coupling to oxygen modes across the cuprates". In: *Phys. Rev. B* 82 (6 Aug. 2010), p. 064513. DOI: 10.1103/PhysRevB.82.064513. URL: https://link.aps.org/doi/10.1103/PhysRevB.82.064513.

[66] C.-C. Kao et al. "X-ray resonant Raman scattering in NiO: Resonant enhancement of the charge-transfer excitations". In: *Phys. Rev. B* 54 (23 Dec. 1996), pp. 16361–16364. DOI: 10.1103/PhysRevB.54.16361. URL: https://link.aps.org/doi/10.1103/PhysRevB.54.16361.

[67] B. Keimer et al. "From quantum matter to high-temperature superconductivity in copper oxides". In: *Nature* 518.7538 (Feb. 2015), pp. 179–186. DOI: 10.1038/nature14165. URL: https://doi.org/10.1038/nature14165.

[68] B. C. Larson et al. "Nonresonant Inelastic X-Ray Scattering and Energy-Resolved Wannier Function Investigation of $d-d$ Excitations in NiO and CoO". In: *Phys. Rev. Lett.* 99 (2 July 2007), p. 026401. DOI: 10.1103/PhysRevLett.99.026401. URL: https://link.aps.org/doi/10.1103/PhysRevLett.99.026401.

[69] T. Learmonth et al. "Resonant soft x-ray inelastic scattering and soft x-ray emission study of the electronic structure of α-MoO_3". In: *Phys. Rev. B* 79 (3 Jan. 2009), p. 035110. DOI: 10.1103/PhysRevB.79.035110. URL: https://link.aps.org/doi/10.1103/PhysRevB.79.035110.

[70] A. G. Loeser et al. "Excitation Gap in the Normal State of Underdoped Bi2Sr2CaCu2O8delta". In: *Science* 273.5273 (July 1996), pp. 325–329. DOI: 10.1126/science.273.5273.325. URL: https://doi.org/10.1126/science.273.5273.325.

[71] Jan Lüning and Coryn Frank Hague. "Resonant Inelastic X-ray Scattering: From band mapping to inter-orbital excitations". In: *Comptes Rendus Physique* 9.5-6 (June 2008), pp. 537–549. DOI: 10.1016/j.crhy.2007.05.020. URL: https://doi.org/10.1016/j.crhy.2007.05.020.

[72] D. S. Marshall et al. "Unconventional Electronic Structure Evolution with Hole Doping inBi2Sr2CaCu2O8: Angle-Resolved Photoemission Results". In: *Physical Review Letters* 76.25 (June 1996), pp. 4841–4844. DOI: 10.1103/physrevlett.76.4841. URL: https://doi.org/10.1103/physrevlett.76.4841.

[73] S. Martin et al. "Normal-state transport properties of $Bi_{2+x}Sr_{2-y}CuO_{6+\delta}$ crystals". In: *Phys. Rev. B* 41 (1 Jan. 1990), pp. 846–849. DOI: 10.1103/PhysRevB.41.846. URL: https://link.aps.org/doi/10.1103/PhysRevB.41.846.

[74] Alberto Martinelli, Fabio Bernardini, and Sandro Massidda. "The phase diagrams of iron-based superconductors: Theory and experiments". In: *Comptes Rendus Physique* 17.1-2 (Jan. 2016), pp. 5–35. DOI: 10.1016/j.crhy.2015.06.001. URL: https://doi.org/10.1016/j.crhy.2015.06.001.

[75] W. Meissner and R. Ochsenfeld. "Ein neuer Effekt bei Eintritt der Supraleitfhigkeit". In: *Die Naturwissenschaften* 21.44 (Nov. 1933), pp. 787–788. DOI: 10.1007/bf01504252. URL: https://doi.org/10.1007/bf01504252.

[76] A. Mesaros et al. "Topological Defects Coupling Smectic Modulations to Intra-Unit-Cell Nematicity in Cuprates". In: *Science* 333.6041 (July 2011), pp. 426–430. DOI: 10.1126/science.1201082. URL: https://doi.org/10.1126/science.1201082.

[77] H. Miao et al. "Incommensurate Phonon Anomaly and the Nature of Charge Density Waves in Cuprates". In: *Phys. Rev. X* 8 (1 Jan. 2018), p. 011008. DOI: 10.1103/PhysRevX.8.011008. URL: https://link.aps.org/doi/10.1103/PhysRevX.8.011008.

[78] MoxFire. *Vectorization of Raman energy level*. 2016. URL: https://upload.wikimedia.org/wikipedia/commons/4/41/Raman_energy_levels.svg.

[79] Joseph Nordgren. "Soft X-Ray Emission Spectroscopy Using Synchrotron Radiation". In: *New Directions in Research with Third-Generation Soft X-Ray Synchrotron Radiation Sources*. Springer Netherlands, 1994, pp. 189–202. DOI: 10.1007/978-94-011-0868-3_7. URL: https://doi.org/10.1007/978-94-011-0868-3_7.

[80] M. R. Norman et al. "Destruction of the Fermi surface in underdoped high-Tc superconductors". In: *Nature* 392.6672 (Mar. 1998), pp. 157–160. DOI: 10.1038/32366. URL: https://doi.org/10.1038/32366.

[81] Kazuki Ohishi et al. "Magnetic Phase Diagram of Hole-Doped Ca2-xNaxCuO2Cl2Cuprate Superconductor". In: *Journal of the Physical Society of Japan* 74.9 (Sept. 2005), pp. 2408–2412. DOI: 10.1143/jpsj.74.2408. URL: https://doi.org/10.1143/jpsj.74.2408.

[82] Y. Ohta, T. Tohyama, and S. Maekawa. "Apex oxygen and critical temperature in copper oxide superconductors: Universal correlation with the stability of local singlets". In: *Phys. Rev. B* 43 (4 Feb. 1991), pp. 2968–2982. DOI: 10.1103/PhysRevB.43.2968. URL: https://link.aps.org/doi/10.1103/PhysRevB.43.2968.

[83] Kozo Okada and Akio Kotani. "Momentum-Specified OxygenKResonant Inelastic X-ray Scattering for Cuprates". In: *Journal of the Physical Society of Japan* 76.12 (Dec. 2007), p. 123706. DOI: 10.1143/jpsj.76.123706. URL: https://doi.org/10.1143/jpsj.76.123706.

[84] H. Kamerlingh Onnes. "Further experiments with liquid helium. C. On the change of electric resistance of pure metals at very low temperatures etc. IV. The resistance of pure mercury at helium temperatures". In: *Through Measurement to Knowledge: The Selected Papers of Heike Kamerlingh Onnes 1853–1926*. Ed. by Kostas Gavroglu and

Yorgos Goudaroulis. Dordrecht: Springer Netherlands, 1991, pp. 261–263. DOI: 10.1007/978-94-009-2079-8_15. URL: https://doi.org/10.1007/978-94-009-2079-8_15.

[85] D. Pelc et al. "Unusual behavior of cuprates explained by heterogeneous charge localization". In: *Science Advances* 5.1 (Jan. 2019), eaau4538. DOI: 10.1126/sciadv.aau4538. URL: https://doi.org/10.1126/sciadv.aau4538.

[86] S. Peli et al. "Mottness at finite doping and charge instabilities in cuprates". In: *Nature Physics* 13.8 (May 2017), pp. 806–811. DOI: 10.1038/nphys4112. URL: https://doi.org/10.1038/nphys4112.

[87] P. M. Platzman and E. D. Isaacs. "Resonant inelastic x-ray scattering". In: *Phys. Rev. B* 57 (18 May 1998), pp. 11107–11114. DOI: 10.1103/PhysRevB.57.11107. URL: https://link.aps.org/doi/10.1103/PhysRevB.57.11107.

[88] Pia Jensen Ray. "Master's thesis: Structural investigation of La(2-x)Sr(x)CuO(4+y) - Following staging as a function of temperature". In: (2016). DOI: 10.6084/M9.FIGSHARE.2075680.V2. URL: https://figshare.com/articles/thesis/Structural_investigation_of_La_2_x_Sr_x_CuO_4_y_Following_staging_as_a_function_of_temperature/2075680/2.

[89] Arpaia Riccardo. "$YBa_2Cu_3O_{7-\delta}$ nanowires to study nanoscale ordering in High-T_C Superconductors". Apr. 2016.

[90] Matteo Rossi et al. "Experimental Determination of Momentum-Resolved Electron-Phonon Coupling". In: *Phys. Rev. Lett.* 123 (2 July 2019), p. 027001. DOI: 10.1103/PhysRevLett.123.027001. URL: https://link.aps.org/doi/10.1103/PhysRevLett.123.027001.

[91] Jean-Pascal Rueff and Abhay Shukla. "Inelastic x-ray scattering by electronic excitations under high pressure". In: *Rev. Mod. Phys.* 82 (1 Mar. 2010), pp. 847–896. DOI: 10.1103/RevModPhys.82.847. URL: https://link.aps.org/doi/10.1103/RevModPhys.82.847.

[92] M Moretti Sala et al. "Energy and symmetry of dd excitations in undoped layered cuprates measured by CuL3resonant inelastic x-ray scattering". In: *New Journal of Physics* 13.4 (Apr. 2011), p. 043026. DOI: 10.1088/1367-2630/13/4/043026. URL: https://doi.org/10.1088/1367-2630/13/4/043026.

[93] D.J. Scalapino and S.R. White. "Stripe structures in the t–t′-J model". In: *Physica C: Superconductivity* 481 (Nov. 2012), pp. 146–152. DOI: 10.1016/j.physc.2012.04.004. URL: https://doi.org/10.1016/j.physc.2012.04.004.

[94] J. Schlappa et al. "Collective Magnetic Excitations in the Spin Ladder $Sr_{14}Cu_{24}\mathbf{O}_{41}$ Measured Using High-Resolution Resonant Inelastic X-Ray Scattering". In: *Phys. Rev. Lett.* 103 (4 July 2009), p. 047401. DOI: 10.1103/PhysRevLett.103.047401. URL: https://link.aps.org/doi/10.1103/PhysRevLett.103.047401.

[95] Simon Schreck et al. "Ground state potential energy surfaces around selected atoms from resonant inelastic x-ray scattering". In: *Scientific Reports* 6.1 (Jan. 2016). DOI: 10.1038/srep20054. URL: https://doi.org/10.1038/srep20054.

[96] Winfried Schülke. *Electron Dynamics by Inelastic X-Ray Scattering*. Oxford series on synchrotron radiation. Oxford: Oxford Univ. Press, 2007. URL: https://cds.cern.ch/record/1058527.

[97] U. Schwingenschlögl, C. Schuster, and R. Frésard. "Electronic structure of a striped nickelate studied by the exact exchange for correlated electrons (EECE) approach". In: *EPL (Europhysics Letters)* 88.6 (Dec. 2009), p. 67008. DOI: 10.1209/0295-5075/88/67008. URL: https://doi.org/10.1209/0295-5075/88/67008.

[98] Götz Seibold et al. "Strange metal behaviour from charge density fluctuations in cuprates". In: *Communications Physics* 4.1 (Jan. 2021). ISSN: 2399-3650. DOI: 10.1038/s42005-020-00505-z. URL: http://dx.doi.org/10.1038/s42005-020-00505-z.

[99] E. H. da Silva Neto et al. "Ubiquitous Interplay Between Charge Ordering and High-Temperature Superconductivity in Cuprates". In: *Science* 343.6169 (Dec. 2013), pp. 393–396. DOI: 10.1126/science.1243479. URL: https://doi.org/10.1126/science.1243479.

[100] Elliot Snider et al. "Room-temperature superconductivity in a carbonaceous sulfur hydride". In: *Nature* 586.7829 (Oct. 2020), pp. 373–377. DOI: 10.1038/s41586-020-2801-z. URL: https://doi.org/10.1038/s41586-020-2801-z.

[101] W. Tabis et al. "Charge order and its connection with Fermi-liquid charge transport in a pristine high-Tc cuprate". In: *Nature Communications* 5.1 (Dec. 2014). DOI: 10.1038/ncomms6875. URL: https://doi.org/10.1038/ncomms6875.

[102] "The electromagnetic equations of the supraconductor". In: *Proceedings of the Royal Society of London. Series A - Mathematical and Physical Sciences* 149.866 (Mar. 1935), pp. 71–88. DOI: 10.1098/rspa.1935.0048. URL: https://doi.org/10.1098/rspa.1935.0048.

[103] Yoshinori Tokura and Takahisa Arima. "New Classification Method for Layered Copper Oxide Compounds and Its Application to Design of New HighTcSuperconductors". In: *Japanese Journal of Applied Physics* 29.Part 1, No. 11 (Nov. 1990), pp. 2388–2402. DOI: 10.1143/jjap.29.2388. URL: https://doi.org/10.1143/jjap.29.2388.

[104] J. M. Tranquada et al. "Coexistence of, and Competition between, Superconductivity and Charge-Stripe Order in $La_{1.6-x}Nd_{0.4}Sr_xCuO_4$". In: *Phys. Rev. Lett.* 78 (2 Jan. 1997), pp. 338–341. DOI: 10.1103/PhysRevLett.78.338. URL: https://link.aps.org/doi/10.1103/PhysRevLett.78.338.

[105] J. M. Tranquada et al. "Evidence for stripe correlations of spins and holes in copper oxide superconductors". In: *Nature* 375.6532 (June 1995), pp. 561–563. DOI: 10.1038/375561a0. URL: https://doi.org/10.1038/375561a0.

[106] J. M. Tranquada et al. "Evidence for stripe correlations of spins and holes in copper oxide superconductors". In: 375.6532 (June 1995), pp. 561–563. DOI: 10.1038/375561a0.

[107] J. M. Tranquada et al. "Simultaneous Ordering of Holes and Spins in $La_2NiO_{4.125}$". In: *Phys. Rev. Lett.* 73 (7 Aug. 1994), pp. 1003–1006. DOI: 10.1103/PhysRevLett.73.1003. URL: https://link.aps.org/doi/10.1103/PhysRevLett.73.1003.

[108] C. M. Varma et al. "Phenomenology of the normal state of Cu-O high-temperature superconductors". In: *Phys. Rev. Lett.* 63 (18 Oct. 1989), pp. 1996–1999. DOI: 10.1103/PhysRevLett.63.1996. URL: https://link.aps.org/doi/10.1103/PhysRevLett.63.1996.

[109] M. A. van Veenendaal, H. Eskes, and G. A. Sawatzky. "Strong nonlocal contributions to Cu 2p photoelectron spectroscopy". In: *Phys. Rev. B* 47 (17 May 1993), pp. 11462–11469. DOI: 10.1103/PhysRevB.47.11462. URL: https://link.aps.org/doi/10.1103/PhysRevB.47.11462.

[110] M. A. van Veenendaal and G. A. Sawatzky. "Nonlocal screening effects in 2p x-ray photoemission spectroscopy core-level line shapes of transition metal compounds". In: *Phys. Rev. Lett.* 70 (16 Apr. 1993), pp. 2459–2462. DOI: 10.1103/PhysRevLett.70.2459. URL: https://link.aps.org/doi/10.1103/PhysRevLett.70.2459.

[111] Michel van Veenendaal and M. W. Haverkort. "Effective operator for $d--d$ transitions in nonresonant inelastic x-ray scattering". In: *Phys. Rev. B* 77 (22 June 2008), p. 224107. DOI: 10.1103/PhysRevB.77.224107. URL: https://link.aps.org/doi/10.1103/PhysRevB.77.224107.

[112] B. Vignolle et al. "Quantum oscillations in an overdoped high-Tc superconductor". In: *Nature* 455.7215 (Oct. 2008), pp. 952–955. DOI: 10.1038/nature07323. URL: https://doi.org/10.1038/nature07323.

[113] I. M. Vishik et al. "A momentum-dependent perspective on quasiparticle interference in Bi2Sr2CaCu2O8". In: *Nature Physics* 5.10 (Aug. 2009), pp. 718–721. DOI: 10.1038/nphys1375. URL: https://doi.org/10.1038/nphys1375.

[114] E Wahlberg et al. "Restoring the strange metal phase via suppression of charge density waves in an underdoped cuprate superconductor". In: *arXiv preprint arXiv:2009.08398v2* (2020).

[115] W. W. Warren et al. "Cu spin dynamics and superconducting precursor effects in planes above T_c in $YBa_2Cu_3O_{6.7}$". In: *Phys. Rev. Lett.* 62 (10 Mar. 1989), pp. 1193–1196. DOI: 10.1103/PhysRevLett.62.1193. URL: https://link.aps.org/doi/10.1103/PhysRevLett.62.1193.

[116] W. D. Wise et al. "Charge-density-wave origin of cuprate checkerboard visualized by scanning tunnelling microscopy". In: *Nature Physics* 4.9 (July 2008), pp. 696–699. DOI: 10.1038/nphys1021. URL: https://doi.org/10.1038/nphys1021.

[117] M. K. Wu et al. "Superconductivity at 93 K in a new mixed-phase Y-Ba-Cu-O compound system at ambient pressure". In: *Phys. Rev. Lett.* 58 (9 Mar. 1987), pp. 908–910. DOI: 10.1103/PhysRevLett.58.908. URL: https://link.aps.org/doi/10.1103/PhysRevLett.58.908.

[118] Tao Wu et al. "Incipient charge order observed by NMR in the normal state of YBa2Cu3Oy". In: *Nature Communications* 6.1 (Mar. 2015). DOI: 10.1038/ncomms7438. URL: https://doi.org/10.1038/ncomms7438.

[119] Tao Wu et al. "Magnetic-field-induced charge-stripe order in the high-temperature superconductor YBa2Cu3Oy". In: *Nature* 477.7363 (Sept. 2011), pp. 191–194. DOI: 10.1038/nature10345. URL: https://doi.org/10.1038/nature10345.

[120] K. Yamada et al. "Doping dependence of the spatially modulated dynamical spin correlations and the superconducting-transition temperature in $La_{2-x}Sr_xCuO_4$". In: *Phys. Rev. B* 57 (10 Mar. 1998), pp. 6165–6172. DOI: 10.1103/PhysRevB.57.6165. URL: https://link.aps.org/doi/10.1103/PhysRevB.57.6165.

[121] H.-B. Yang et al. "Emergence of preformed Cooper pairs from the doped Mott insulating state in Bi2Sr2CaCu2O8". In: *Nature* 456.7218 (Nov. 2008), pp. 77–80. DOI: 10.1038/nature07400. URL: https://doi.org/10.1038/nature07400.

[122] Hideki Yoshizawa et al. "An Incommensurate Magnetic Diffuse Scattering in Superconducting La1.92Sr0.08CuO4-". In: *Journal of the Physical Society of Japan* 57.11 (Nov. 1988), pp. 3686–3689. DOI: 10.1143/jpsj.57.3686. URL: https://doi.org/10.1143/jpsj.57.3686.

[123] Jan Zaanen and Olle Gunnarsson. "Charged magnetic domain lines and the magnetism of high-T_c oxides". In: *Phys. Rev. B* 40 (10 Oct. 1989), pp. 7391–7394. DOI: 10.1103/PhysRevB.40.7391. URL: https://link.aps.org/doi/10.1103/PhysRevB.40.7391.